iScience

CellPress
OPEN ACCESS

Article

AURKA and PLK1 inhibition selectively and synergistically block cell cycle progression in diffuse midline glioma

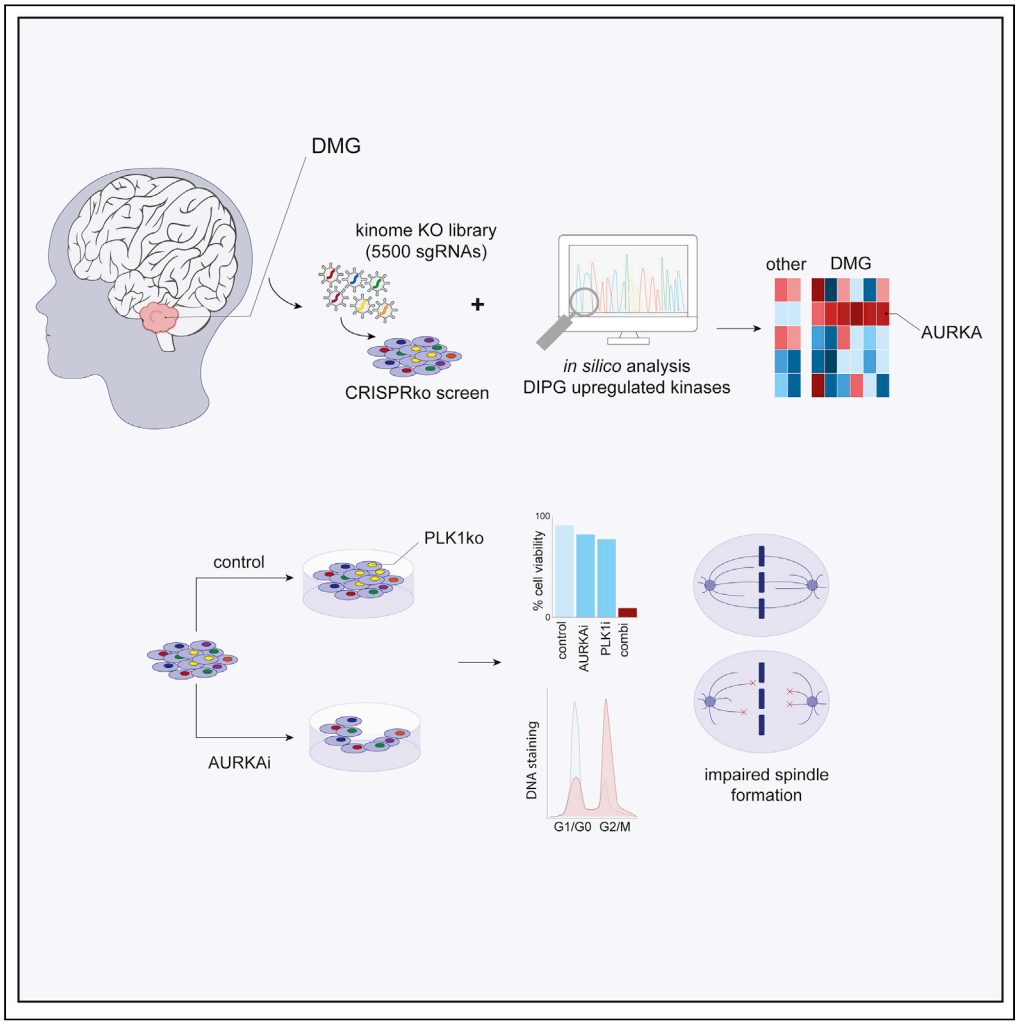

Dennis S. Metselaar, Aimée du Chatinier, Michaël H. Meel, ..., Jan Koster, Gertjan J.L. Kaspers, Esther Hulleman

e.hulleman@prinsesmaximacentrum.nl

Highlights

Kinome-wide CRISPR/Cas9 screening in primary DMG tumoroids

CRISPR screening identifies AURKA as therapeutic target in DMG

AURKA inhibition sensitizes DMG to PLK1 knockout

Combined AURKA and PLK1 inhibition selectively impairs DMG cell division

Metselaar et al., iScience *25*, 104398
June 17, 2022 © 2022 The Author(s).
https://doi.org/10.1016/j.isci.2022.104398

iScience

CellPress
OPEN ACCESS

Article

AURKA and PLK1 inhibition selectively and synergistically block cell cycle progression in diffuse midline glioma

Dennis S. Metselaar,[1,2] Aimée du Chatinier,[1] Michaël H. Meel,[1] Giovanna ter Huizen,[2] Piotr Waranecki,[1] Joshua R. Goulding,[2] Marianna Bugiani,[3] Jan Koster,[4] Gertjan J.L. Kaspers,[1,2] and Esther Hulleman[1,*]

SUMMARY

Diffuse midline gliomas (DMG) are highly malignant incurable pediatric brain tumors. In this study, we show that Aurora kinase A (AURKA) is overexpressed in DMG and can be used as a therapeutic target. Additionally, AURKA inhibition combined with CRISPR/Cas9 screening in DMG cells, revealed polo-like kinase 1 (PLK1) as a synergistic target with AURKA. Using a panel of patient-derived DMG culture models, we demonstrate that treatment with volasertib, a clinically relevant and selective PLK1 inhibitor, synergizes with different AURKA inhibitors, supporting the CRISPR screen results. Mechanistically, our results show that combined loss of PLK1 and AURKA causes a G2/M cell cycle arrest which blocks vital parts of DNA-damage repair and induces apoptosis, solely in DMG cells. Altogether, our findings highlight the importance of AURKA and PLK1 for DMG propagation and demonstrate the potential of concurrently targeting these proteins as a therapeutic strategy for these devastating pediatric brain tumors.

INTRODUCTION

Diffuse midline gliomas (DMG), including diffuse intrinsic pontine gliomas (DIPG), are highly aggressive incurable pediatric brain tumors and are the major cause of death in children suffering from brain tumors (Johung and Monje, 2017). In DMG, the most frequent genetic aberration is a lysine-to-methionine substitution at position 27 in H3.1 (H3.1K27M) or H3.3 (H3.3K27M), which results in altered gene expression and aggressive tumor growth (Buczkowicz et al., 2014; Lowe et al., 2019). Despite advances in understanding the molecular basis of these tumors, the clinical prognosis for patients with DMG has not improved in the past decades (Jones et al., 2017). To this day, focal radiation therapy remains one of the cornerstones of current treatment regimens, although this generally provides only temporary symptom relief and a minor delay in tumor progression (Meel et al., 2018c). As such, DMG tumors are still among the most lethal malignancies in children, and improved therapeutic strategies are desperately needed.

Over the past decade, the molecular background of diffuse midline gliomas has been thoroughly investigated and many DMG *in vitro* and *in vivo* models have been established. This has led to the preclinical identification of many potentially suitable agents and targets for the treatment of this disease. Despite these advances, only a few effective single-agents for the treatment of DMG have been identified in a preclinical setting, such as the MELK inhibitor OTSSP167, the HDAC inhibitor Panobinostat, and the WEE1 inhibitor AZD1775 (Meel et al., 2018a, 2020; Mueller et al., 2018). However, monotherapy often results in recurrent growth from resistant DMG subclones, which has rendered all drugs tested in clinical trials to this day ineffective.

In this study, we searched for combinational therapeutic targets that are essential for DMG survival by conducting an explorative kinome-wide CRISPR/Cas9 screening in primary DMG cultures. Through an additional *in silico* analysis of publicly available gene expression datasets, we found that AURKA, a serine/threonine kinase that acts as a cell cycle regulator during G2/M phase and meiosis (Marumoto et al., 2002), is one of the few kinases that is both highly upregulated in DMG tissues and essential for DMG survival in the CRISPR screens.

AURKA upregulation is common in malignancies and dysregulation has been associated with cancer onset, therapy resistance, and metastasis (Marumoto et al., 2002). Because AURKA plays an important role in

[1]Princess Máxima Center for Pediatric Oncology, Heidelberglaan 25, 3584CS Utrecht, the Netherlands

[2]Emma Children's Hospital, Amsterdam University Medical Centers, Vrije Universiteit Amsterdam, Pediatric Oncology, Cancer Center Amsterdam, Amsterdam, the Netherlands

[3]Department of Pathology, Amstrdam University Medical Centers, Amsterdam, the Netherlands

[4]Department of Oncogenomics, Amsterdam University Medical Centers, University of Amsterdam, Amsterdam, the Netherlands

*Correspondence: e.hulleman@prinsesmaximacentrum.nl

https://doi.org/10.1016/j.isci.2022.104398

This is an open access article under the CC BY-NC-ND license (http://creativecommons.org/licenses/by-nc-nd/4.0/).

Table 1. Top 25 upregulated kinases in DMG[a]

Rank	Gene	Probeset	Fold increase (log2)	Expression increase (log2)	p value (FDR)
1	TOP2A	201,292_at	10.12	7.07	9.76×10^{-57}
2	MELK	204,825_at	4.70	5.89	5.18×10^{-61}
3	BUB1	209,642_at	3.49	4.77	1.75E-40
4	TTK	204,822_at	3.42	4.83	5.87×10^{-42}
5	OSR1	228,399_at	3.20	3.89	1.20E-20
6	PBK	219,148_at	3.12	5.17	4.35×10^{-59}
7	WEE1	212,533_at	2.45	5.21	2.68×10^{-46}
8	GRK7	1,552,929_at	2.08	1.51	3.46×10^{-5}
9	NEK2	204,641_at	1.98	3.33	2.56×10^{-22}
10	STK33	228,035_at	1.93	2.97	2.08×10^{-19}
11	TEX14	221,035_s_at	1.90	2.60	1.64×10^{-13}
12	AURKB	209,464_at	1.75	2.27	2.82E-20
13	BUB1B	203,755_at	1.72	2.85	4.08×10^{-32}
14	HK2	202,934_at	1.62	3.41	2.81×10^{-32}
15	AURKA	204,092_s_at	1.55	2.33	2.68×10^{-32}
16	ROR2	205,578_at	1.55	1.31	6.86×10^{-6}
17	CHEK2	210,416_s_at	1.55	1.92	3.44×10^{-15}
18	PLAU	205,479_s_at	1.54	1.89	2.31×10^{-14}
19	DYRK3	210,151_s_at	1.48	2.04	6.38×10^{-15}
20	MASTL	228,468_at	1.46	1.92	3.69×10^{-47}
21	LCK	204,891_s_at	1.44	1.08	8.95×10^{-6}
22	STK10	203,047_at	1.44	1.73	1.70×10^{-9}
23	STK17A	202,693_s_at	1.39	2.37	3.68×10^{-63}
24	LATS1	227,772_at	1.38	2.28	1.55×10^{-54}
25	MORC4	219,038_at	1.37	1.93	7.71×10^{-41}

[a]Sorted on log2 fold increase. DMG tumor samples (n=27, GSE26576) compared to nonmalignant brain tissues (n=174, GSE11882) including 2 nonmalignant pediatric brain stem tissues (GSE26576).

chromosomal alignment and spindle formation during mitosis, and cancer cells tend to be more mitotically active than their healthy counterpart cells, AURKA upregulation in cancer is not surprising. However, inhibition of AURKA has only been shown effective in selective malignancies, indicating that many cancers do not fully rely on AURKA for mitosis (Du et al., 2021). Furthermore, in several cancers, AURKA has been shown to play a vital role in the epithelial-to-mesenchymal transition, which has been described as an essential mechanism for tumor survival in DMG (Yang et al., 2016).

Using additional CRISPR/Cas9 screening in the presence of an AURKA inhibitor, we identified the proto-onco cell cycle regulator PLK1 as synergistic drug target with AURKA inhibition in our primary patient-derived DMG models. In this study, we further establish and investigate this AURKA/PLK1 inhibition method as a multi-drug preclinical therapeutic target for the treatment of DMG.

RESULTS

CRISPR/Cas9 screening and *in silico* analysis identify AURKA as potential drug target in DMG

To identify novel therapeutic targets in DMG, we performed an explorative kinome-wide CRISPR/Cas9 inducible knockout screen in two primary pediatric DMG models (VUMC-DIPG-10 and HSJD-DIPG-07). Through the MAGeCK-VISPR bioinformatics pipeline, we identified negatively and positively selected subclones at 14 and 21 days post knockout. To test which negatively selected kinases correlate with up-regulation of their respective genes in a DMG patient pool, we performed an *in silico* analysis of kinase mRNA expression profiles from patients with DMG and compared these to nonmalignant brain tissues, including healthy brainstem (Table 1). Several lethal hits from the CRISPR/Cas9 screen correlated with

CellPress
OPEN ACCESS

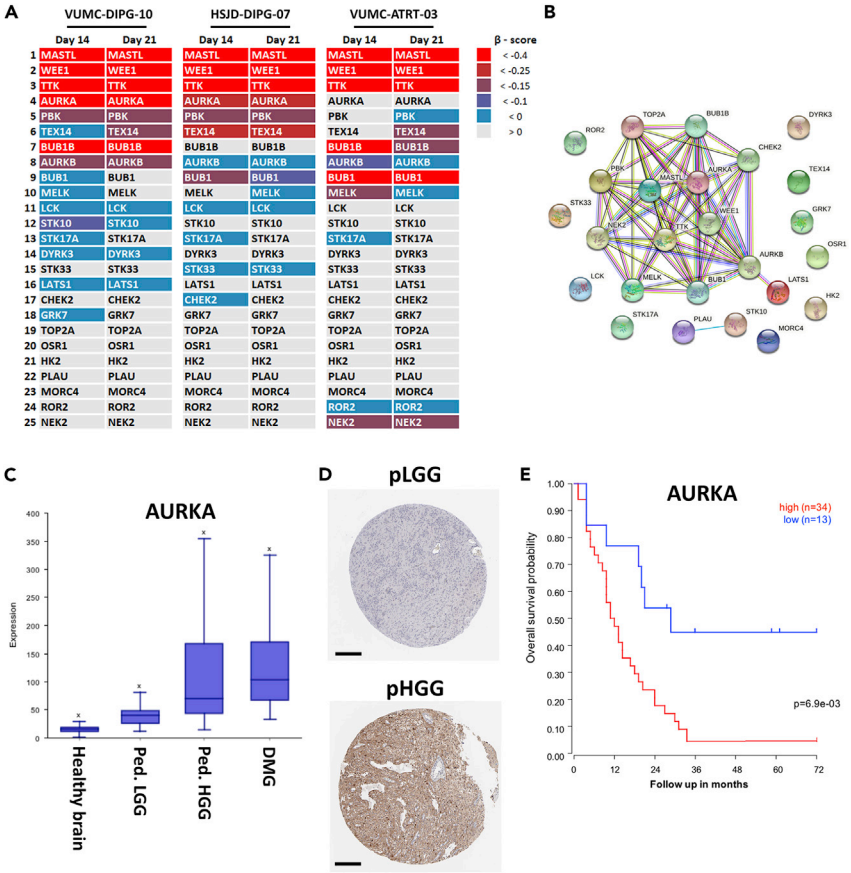

Figure 1. *In silico* analysis and CRISPR screening identify AURKA as potential drug target in DMG

(A) Top upregulated genes in DMG ordered by their importance for DMG cell survival as identified through the kinome-wide CRISPR/Cas9 screen. Screening was performed in VUMC-DIPG-10, HSJD-DMG07, and VUMC-ATRT-03 cells and analyzed at 14 and 21 days after knockout. Red squares represent essential genes for cell survival while knockout of genes indicated in gray did not have any effect in the CRISPR screen. Color cutoff is indicated in Figure S1.

(B) STRING protein interaction analysis of the 25 strongest upregulated kinases in DMG. Each colored line indicates interaction between both adjacent proteins, as further explained at http://string-db.org.

(C) mRNA expression levels of AURKA in healthy brain tissues (n = 172, GSE11882) (Berchtold et al., 2008), pediatric low-grade glioma tissues (n = 10, GSE26576), pediatric high-grade glioma tissues (n = 53, GSE19578), and DMG tissues (n = 27, GSE26576) (Paugh et al., 2011).

(D) Immunohistochemical staining of AURKA (brown) in brain tumor biopsy samples. Upper image depicts tumor tissue from a pediatric low-grade glioma (patient ID: 158, www.proteinatlas.org) and the lower image depicts tumor tissue from a pediatric high-grade glioma (patient ID: 1599, www.proteinatlas.org). Scale bar length is 400 μm.

(E) Kaplan-Meijer curve depicting survival of 47 patients with pHGG with high (red) or low (blue) AURKA mRNA expression (expression cut-off: 48.7) (GSE: 19578) (Paugh et al., 2010). Survival differences between groups were tested using the log rank (Mantel-Cox) test.

upregulation in DMG tissues, as visualized in Figure 1A. Knockout of the chromosomal alignment regulators AURKA, MASTL, WEE1, and TTK caused the most significant negative selection both at day 14 and 21 in both DMG models and are also highly upregulated in DMG tumor samples. Intriguingly, in a control CRISPR/Cas9 screening in non-DMG pediatric brain tumor cells (VUMC-ATRT-03), MASTL, WEE1, and TTK knockout also caused cell death, whereas AURKA knockout did not affect cell viability. Because this effect was observed solely in our DMG models, we hypothesized an essential role for AURKA specifically in DMG cells. From the top 25 upregulated kinases in DMG, 12 have a proven interaction with AURKA, as denoted in the STRING protein interaction algorithm (http://string-db.org/) (Figure 1B). These interacting kinases are all involved in mitotic regulation and include the strongest lethal hits in the DMG CRISPR/Cas9 screen.

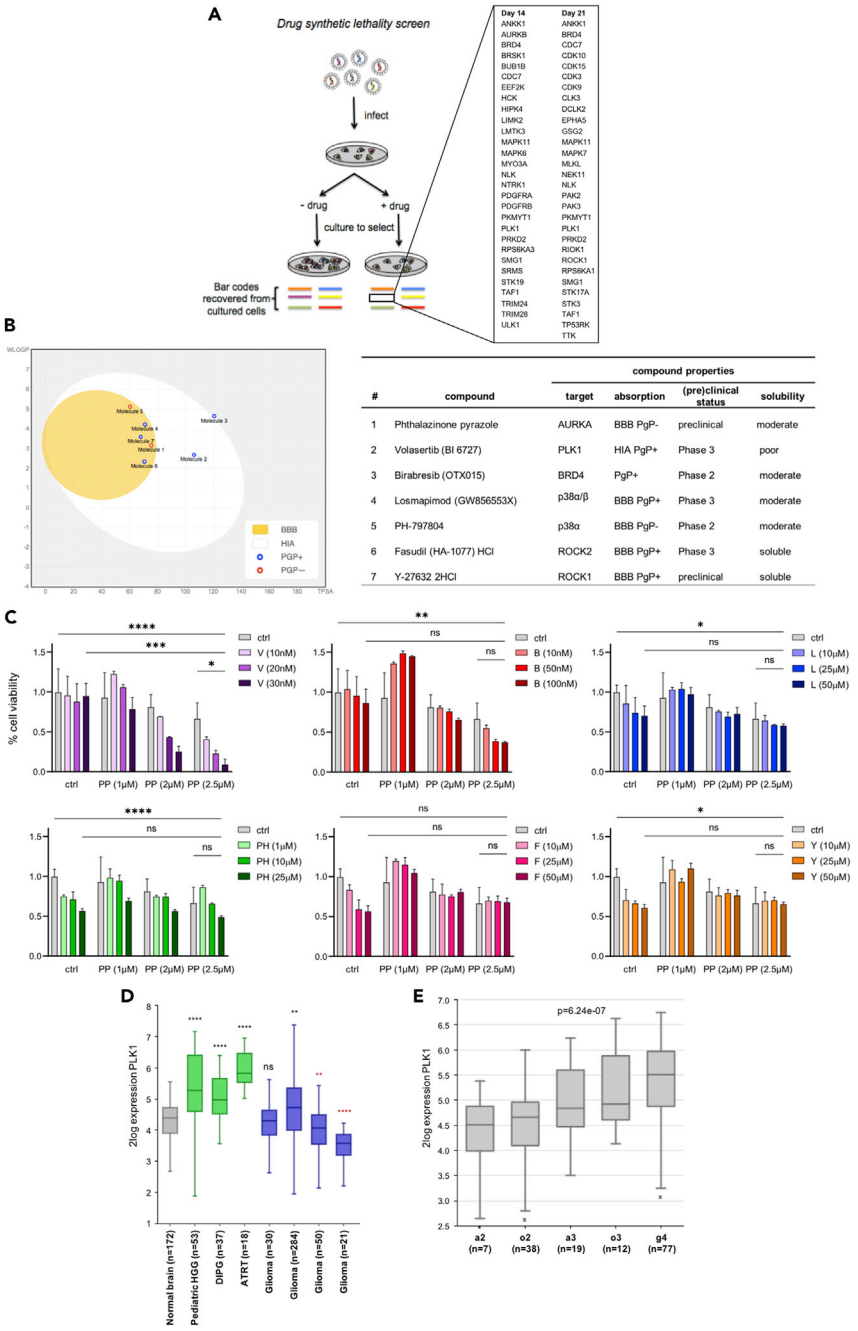

#	compound	compound properties: target	absorption	(pre)clinical status	solubility
1	Phthalazinone pyrazole	AURKA	BBB PgP-	preclinical	moderate
2	Volasertib (BI 6727)	PLK1	HIA PgP+	Phase 3	poor
3	Birabresib (OTX015)	BRD4	PgP+	Phase 2	moderate
4	Losmapimod (GW856553X)	p38α/β	BBB PgP+	Phase 3	moderate
5	PH-797804	p38α	BBB PgP-	Phase 2	moderate
6	Fasudil (HA-1077) HCl	ROCK2	BBB PgP+	Phase 3	soluble
7	Y-27632 2HCl	ROCK1	BBB PgP+	preclinical	soluble

Figure 2. Identification of PLK1 as a therapeutic target to strengthen AURKA inhibition in DMG

(A) Schematic representation of the CRISPR/Cas9 synthetic lethality screen, representing kinase knockouts that were negatively selected after 14 (left) and 21 (right) days with phthalazinone pyrazole treatment compared to non-treated conditions across two DMG models and one ATRT model (VUMC-DIPG-10, HSJD-DIPG-07, and VUMC-ATRT-03).

(B) *In silico* calculated brain penetrating abilities of the selected compounds (left), using the Brain Or IntestinaL EstimateD permeation (BOILED-Egg) method (www.swissadme.ch/index.php) (Daina and Zoete, 2016), and a summary of the selected compounds including their targets, respective clinical status, and solubility (right). The white and yellow regions in the BOILED-Egg analysis indicate the molecules with the highest probability of being absorbed by the gastrointestinal tract (HIA) and to permeate to the blood-brain barrier (BBB), respectively. Compounds with good (+) and poor (−) substrate binding to p-glycoprotein (PgP) are depicted in blue and red, respectively.

(C) Bar graphs visualizing cell viability of SU-DIPG-IV cells after 96 h treatment with volasertib (V), birabresib (B), losmapimod (L), PH-797804 (PH), fasudil (F), or Y-27632 (Y) at the indicated concentrations as monotherapy and in combination

CellPress
OPEN ACCESS

Figure 2. *Continued*

with 1, 2, or 2.5μM phthalazinone pyrazole (PP). Data represented as percentage viability compared to untreated controls, average ±SD (n = 3). ns = not significant, *p < 0.05, **p < 0.01, ***p < 0.001, ****p < 0.0001 (one-way ANOVA and post-hoc unpaired, two-tailed student's t-tests with Bonferroni correction).

(D) PLK1 mRNA (log2) expression levels in healthy brain tissues (gray) compared to pHGG, DMG, and ATRT (green) and adult mixed and high-grade glioma datasets (blue) (GSE in order: 11882 (Berchtold et al., 2008), 19578 (Paugh et al., 2010), 26576 (Paugh et al., 2011), 28026 (Birks et al., 2011) (Gleize et al., 2015), 16011 (Gravendeel et al., 2009), 43378 (Kawaguchi et al., 2013), 50774 (Zhang et al., 2014), 7696 (Murat et al., 2008), and 4290 (Sun et al., 2006)). Significance of each dataset compared to healthy brain, with upregulation in black and downregulation in red. ns = not significant, **p < 0.01, ***p < 0.001, ****p < 0.0001 (one-way ANOVA).

(E) PLK1 (log2) mRNA expression levels compared between gliomas of different grades (GSE: 4290) (Sun et al., 2006). o2 = oligodendroglioma grade 2, o3 = oligodendroglioma grade 3, a2 = astrocytoma grade 2, a3 = astrocytoma grade 3, g4 = glioblastoma grade 4. Overall mRNA expression differences between groups were tested using ANOVA. Figures 2D and 2E were generated using the R2 platform (http://r2.amc.nl).

Further analysis in patient-derived expression datasets show that *AURKA* is specifically overexpressed in pediatric high-grade gliomas (pHGG)—of which DMG is a smaller subgroup—while pediatric lower grade gliomas (pLGG) only show minor elevated *AURKA* expression (Figure 1C). Subsequently, this also translates into a dramatic differential protein expression between low and high-grade pediatric gliomas (Figure 1D). Furthermore, in a population of 47 patients with pHGG, high *AURKA* expression in the tumor has a significantly (p = 0.0069) worse prognosis over lower expression (Figure 1E). In conclusion, these results indicate that DMGs, in contrast to healthy brain or lower grade tumor tissues, highly depend on AURKA expression, which may therefore serve as a relevant therapeutic target.

CRISPR/Cas9 screening identifies PLK1 as a therapeutic target to strengthen AURKA inhibition in DMG

High-grade pediatric brain tumors are known for their ability to escape drug treatment through clonal evolution of therapy resistant tumor subclones. Therefore, we aimed to identify synthetic lethal combinations by conducting another CRISPR/Cas9 screen in the presence of the highly selective AURKA inhibitor phthalazinone pyrazole (PP) (Prime et al., 2011) in the models that were also used in the explorative CRISPR screen. From this CRISPR/Cas9 synthetic lethality screen, we selected kinase knockouts that significantly reduced growth rate in the presence of PP treatment after 14 and 21 days (Figures 2A and S2). By exploring their function and associated signaling pathways using the STRING protein interaction algorithm, and gene ontology analysis, we identified three main pathways: the mitotic spindle/cell cycle checkpoint pathway, the p38 pathway, and the Rho signaling pathway. We selected a panel of inhibitors against kinases with a prominent function within these pathways and other clinically relevant drug targets, with each compound chosen based on target selectivity, clinical status, and an *in silico* pharmacokinetic analysis (Figure 2B). We then investigated synergism of these compounds with PP by assessing cell viability in three DMG models and found that PP synergized most significantly with the PLK1 inhibitor volasertib, with less than 10% cell survival after treatment with the combination therapy (Figure 2C). Based on these results, PLK1 was selected for further evaluation. Notably, when analyzing *PLK1* expression in publicly available gene expression datasets using the online bioinformatics tool R2 (http://r2.amc.nl), we noticed strong *PLK1* upregulation in pediatric brain tumor datasets while these tumors in adults did not show any *PLK1* upregulation or even significant downregulation compared to healthy brain tissues (Figure 2D), which may suggest specific efficacy of the proposed treatment strategy in pediatric patients. Furthermore, as with *AURKA*, *PLK1* is more significantly overexpressed in pHGG compared to their lower grade counterparts (Figure 2E). Additionally, in autopsy-derived pediatric DMG tissues, we confirmed AURKA and PLK1 protein upregulation in the tumor cells compared to neighboring nonmalignant brain cells (Figure S3).

Combined inhibition of AURKA and PLK1 synergistically reduces growth and viability in DMG neurosphere models

To validate if AURKA inhibition indeed synergizes with PLK1 inhibition, we combined PP treatment with the clinically used PLK1 inhibitor volasertib in a panel of six patient-derived DMG cultures and one pediatric glioblastoma (GBM) culture. By measuring cell viability after 96 h of treatment at different concentrations, based on single-drug response (Figure 3A), we created a synergy matrix which shows strong synergism between PP and volasertib in five of the models (JHH-DIPG-01, HSJD-DIPG-07, SU-DIPG-IV, SU-DIPG-XXI, and SU-pcGBM-02), while two other models (VUMC-DIPG-10 and VUMC-DIPG-G) show no or limited synergism (Figures 3B and S5). Subsequently, we studied if this synergy would be maintained over a longer

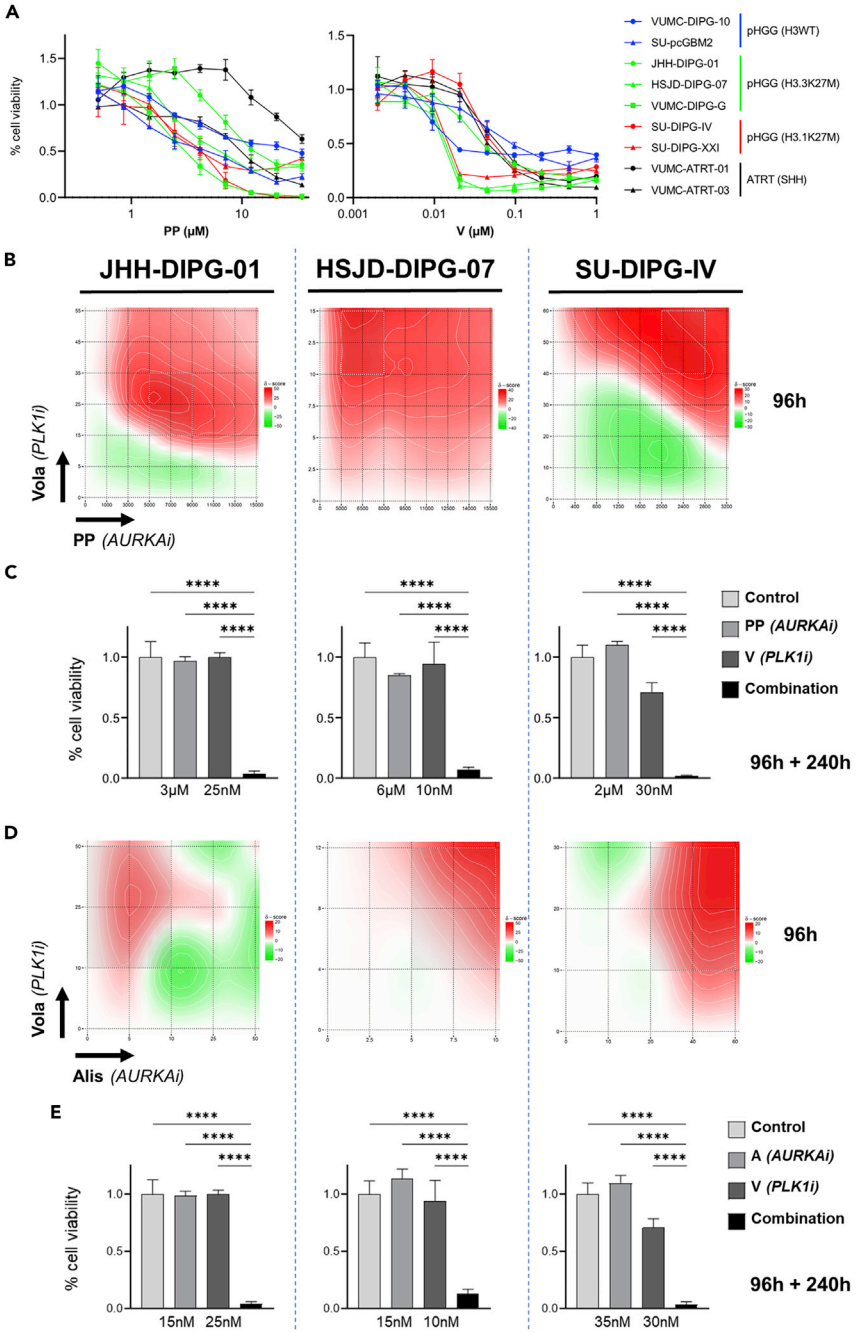

Figure 3. Combined inhibition of AURKA and PLK1 reduces growth and viability in DMG neurosphere models

(A) Dose-response curves representing cell viability in all culture models used in this manuscript after 96 h treatment with phthalazinone pyrazole (PP) (left) or volasertib (V) (right). Histone H3-wildtype (H3WT) DMG models are depicted in blue, DMG models with lysine-to-methionine substitution at histone H3.3 (H3.3K27M) in green, DMG models with lysine-to-methionine substitution at histone H3.1 (H3.1K27M) in red, and sonic hedgehog (SHH) subtype ATRT models in black. Data represented as percentage viability compared to untreated controls, average ±SD (n = 3).

(B) 2D visualization of synergy between phthalazinone pyrazole (PP) and volasertib (V) at various concentrations in three different primary DMG cultures (96 h treatment). Synergy scores are based on the average cell viability at the indicated concentrations and were calculated using the zero interaction potency (ZIP) model of the SynergyFinder software (http://synergyfinder.fimm.fi) (29, 30). ZIP synergy scores >0 indicate synergism (in red) and <0 indicate anti-synergism (in green). ZIP scores >20 indicate strong synergism.

CellPress
OPEN ACCESS

Figure 3. *Continued*

(C) Bar graphs visualizing long-term cell viability after treatment with phthalazinone pyrazole (PP), volasertib (V), or a combination thereof (96 h treatment +240h recovery). ****p < 0.0001 (one-way ANOVA and post-hoc unpaired, two-tailed student's t-tests with Bonferroni correction).

(D) 2D visualization of synergy between alisertib (A) and volasertib (V) at various concentrations in three different primary DMG cultures (96 h treatment). Synergy scores are based on the average cell viability at the indicated concentrations and were calculated using the zero interaction potency (ZIP) model of the SynergyFinder software (http://synergyfinder.fimm.fi) (29, 30). ZIP synergy scores above 0 indicate synergism (in red) and below 0 indicate anti-synergism (in green).

(E) Bar graphs visualizing long-term cell viability after treatment with alisertib (A), volasertib (V), or a combination thereof (96 h treatment +240h recovery). ****p < 0.0001 (one-way ANOVA and post-hoc unpaired, two-tailed student's t-tests with Bonferroni correction).

period by performing long-term cell-viability assays. After 96 h of treatment followed by 10 days of recovery in fresh media, we observed even stronger synergism between PP and volasertib (Figure 3C), except in the two non-responder models which still lacked synergy (Figure S5). To test if AURKA/PLK1 inhibition indeed acts as a tumor-specific treatment strategy in DMG cells, we looked for PP with volasertib treatment synergism in primary human astrocytes. Using combinations of all PP and volasertib concentrations used in this study, we did not observe any elevated toxicity or significant synergy between the two compounds in primary human astrocytes (Figure S6).

To confirm that PP acquires its antitumor synergism with volasertib through inhibition of AURKA, we conducted short- and long-term viability assays in our DMG models using the highly specific AURKA inhibitor alisertib in combination with volasertib. Similar to PP, low nanomolar concentrations of alisertib significantly enhanced the efficacy of volasertib after 96 h in all cultures, except VUMC-DIPG-10 and VUMC-DIPG-G (Figures 3D and S7). Also, long-term, responder and non-responder models fully converged with those observed for PP, confirming that treatment synergism with volasertib can be recapitulated with other AURKA inhibitors (Figures 3E and S7).

Stable AURKA or PLK1 knockdown mimics phthalazinone pyrazole and volasertib inhibitor sensitivity in DMGs

To exclude potential off-target effects of the inhibitors used in our experiments, we established stable AURKA and PLK1 knockdown in patient-derived DMG cultures through lentiviral shRNA transduction. To find optimal knockdown conditions, we used three different shRNAs per gene to establish multiple knockdown clones per culture. We used the cell lines with the strongest knockdown, as confirmed in VUMC-DIPG-10, JHH-DIPG-01, HSJD-DIPG-07, and SU-DIPG-IV, using western blot analysis (Figure 4A). AURKA and PLK1 knockdown cells were treated for 96 h with volasertib and PP, respectively, and cell viability was compared to treatment in empty-vector control cells. AURKA knockdown increased volasertib sensitivity significantly in all DMG knockdown cells (Figure 4B). Reversely, PLK1 knockdown significantly increased PP sensitivity in all DMG knockdown cells (Figure 4B). To test if AURKA inhibition combined with PLK1 inhibition might also be relevant in another type of aggressive pediatric brain tumor, we established PLK1 and AURKA knockdown in two primary ATRT culture models. Strikingly, both ATRT knockdown models did not show any increased sensitivity to PP and volasertib treatment (Figure S8), suggesting that synergy from AURKA with PLK1 inhibition is specific to DMG.

AURKA/PLK1 protein expression as predictor for AURKA/PLK1 inhibitor sensitivity

Previous studies have shown that the degree of AURKA or PLK1 expression is predictive for the cytotoxic effect of inhibition of these proteins (Li et al., 2015a; Spartà et al., 2014). Therefore, we analyzed AURKA and PLK1 protein expression in our DMG and GBM models using western blot analysis. While our two best responder models (SU-DIPG-IV and JHH-DIPG-01) showed elevated levels of both AURKA and PLK1, we did not observe a further correlation between baseline expression and treatment sensitivity (Figure 5A). However, analysis of protein expression after treatment with PP demonstrated that all five responder models (as defined in Figures S5 and S7) show upregulated AURKA protein expression upon treatment, while the two non-responder models (VUMC-DIPG-G and VUMC-DIPG-10) maintain low AURKA expression after PP treatment (Figure 5B). Taken together, these results might suggest that PP/volasertib treatment sensitivity correlates with AURKA expression after treatment, indicating that its expression might serve as predictive biomarker. However, additional research is necessary to confirm these findings.

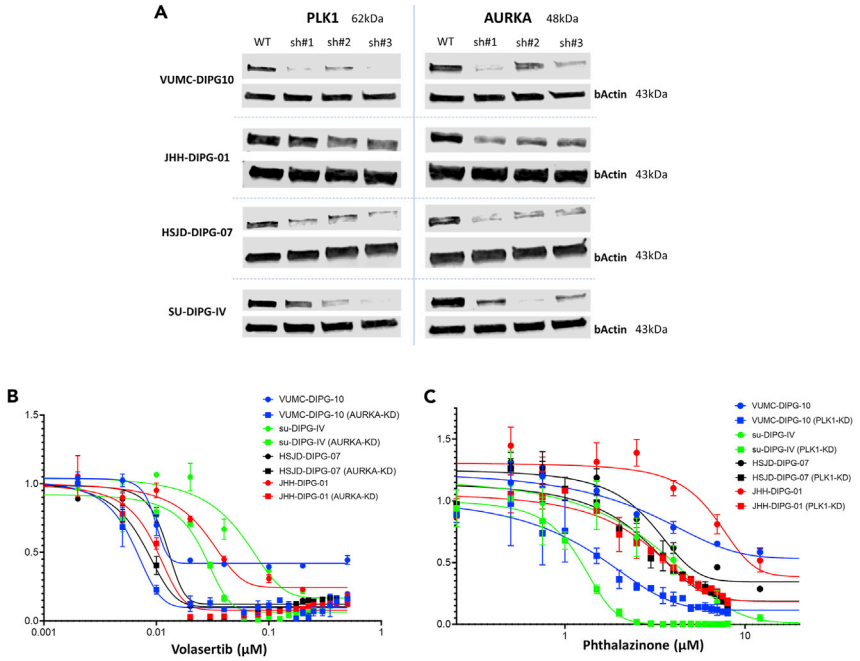

Figure 4. AURKA knockdown induces volasertib sensitivity while reversely PLK1 knockdown causes phthalazinone pyrazole sensitivity in DMG cells

(A) Western blot analysis showing PLK1 expression in shRNA-control and PLK1-shRNA expressing DMG cells (left) and AURKA expression in shRNA-control and AURKA-shRNA expressing DMG cells (right).

(B) Dose-response curves illustrating the cytotoxic effect of volasertib in empty vector versus AURKA-shRNA expressing DMG cells (left) and PP in empty vector versus PLK1-shRNA expressing DMG cells (right). Viability-curves depicting circles represent empty vector cells while squares indicate knockdown. Error bars indicate SD.

Combined inhibition of AURKA and PLK1 impairs cell division and induces DNA damage in DMG cells with AURKA/PLK1 overexpression

To elucidate the molecular mechanisms by which increased AURKA/PLK1 expression confers a better therapeutic response to PP and volasertib, we investigated differential mRNA expression between pHGG tissue samples with high and low *AURKA*/*PLK1* expression in a publicly available expression dataset. T-distributed stochastic neighbor embedding (t-SNE) analysis indicated that pHGG tumor samples with high or low *AURKA* expression form distinct subgroups based on their genome-wide mRNA expression profiles (Figure 6A). Furthermore, unsupervised hierarchical clustering analysis of differentially expressed genes between tumor samples with high and low *AURKA* expression revealed two distinct expression profiles (Figure 6B). Additionally, we observed that *AURKA* and *PLK1* expression levels correlate with each other ($r = 0.850$; $p = 7.95 \times 10^{-16}$) (Figure 6C). These results suggest that tumors with overexpression of AURKA and PLK1 have a distinct expression profile compared to their lower expressing counterparts. We analyzed these differential expression profiles, by conducting gene ontology analyses, and found a significant enrichment of gene signatures related to chromosome segregation and mitosis in the group of genes selectively overexpressed in pHGG with the highest *AURKA* expression (cutoff: FDR-corrected p value $\leq 10^{-32}$) (Figure 6D). These results suggest that pHGG, including DMG, with overexpression of AURKA and PLK1 are specifically dependent on these and other mitotic regulators and that inhibition of these proteins renders them incapable of dividing, leading to cell death (Asteriti et al., 2015; Joukov and De Nicolo, 2018; Lens et al., 2010). To further explore this hypothesis in DMG, we treated SU-DIPG-IV cells, which exhibit relatively high AURKA and PLK1 expression, with PP, volasertib, or the combination thereof and visualized cell division by immunofluorescence. We found that treatment with both compounds increased the percentage of multinuclear cells compared to monotherapy, confirming that concomitant inhibition of AURKA and PLK1 impairs cell division in cells with overexpression of AURKA/PLK1 (Figure 7A). Because these multinuclear cells indicate cell cycle arrest in the G2/M phase, we performed a flow cytometry cell cycle analysis in all models used in this study. This cell cycle analysis confirmed that DMG cells are pushed into a complete G2/M arrest after PP and volasertib combination treatment (Figure 7B). Strikingly,

CellPress
OPEN ACCESS

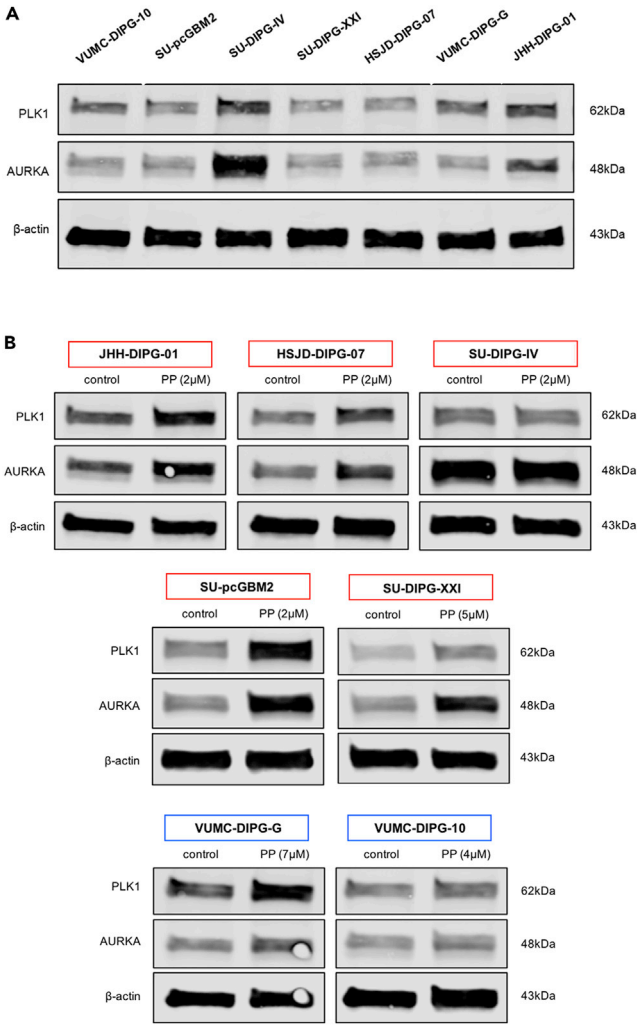

Figure 5. AURKA/PLK1 expression is a potential predictor for AURKA/PLK1 inhibitor sensitivity

(A) Western blot analysis showing baseline expression levels of AURKA and PLK1 in a panel of six primary DMG cultures and one pediatric GBM culture. β-actin was used as a loading control.

(B) Western blot analysis showing AURKA and PLK1 expression in a panel of six primary DMG cultures and one pediatric GBM culture after 24 h treatment with phthalazinone pyrazole (PP) at the indicated concentrations. β-actin was used as a loading control. Responder models are indicated in red and non-responder models in blue, as shown in Figure S4.

the non-responder models (VUMC-DIPG-10 and VUMC-DIPG-G) showed no clear shift into a G2/M arrest, indicating that cell cycle arrest plays a major role in response to our proposed therapeutic strategy (Figure S9).

DNA-damage repair mechanisms are often limited to a specific phase of the cell cycle, and when cells are stuck in G2/M phase, they lose their ability to use non-homologous end-joining (NHEJ) for the repair of DNA double-strand breaks (Zhao et al., 2017). Another way to repair such double-strand breaks is through homologous recombination (HR) which is active during G2 phase (Zhao et al., 2017). However, PLK1 is a regulator of the HR modulator RAD51 through phosphorylation, and we therefore hypothesized that volasertib, through PLK1 inhibition, acts as a double-edged sword when DMG cells are stuck in G2/M phase, by precluding these cells from using yet another mechanism for the repair of DNA breaks (Yata et al., 2012). Therefore, we used western blot to examine the HR-marker RAD51 and found that this protein is depleted from our DMG cultures after PP and volasertib combination therapy, indicating that HR is inhibited (Figure 7C). Subsequently, we show a reverse correlation between RAD51 expression and protein expression

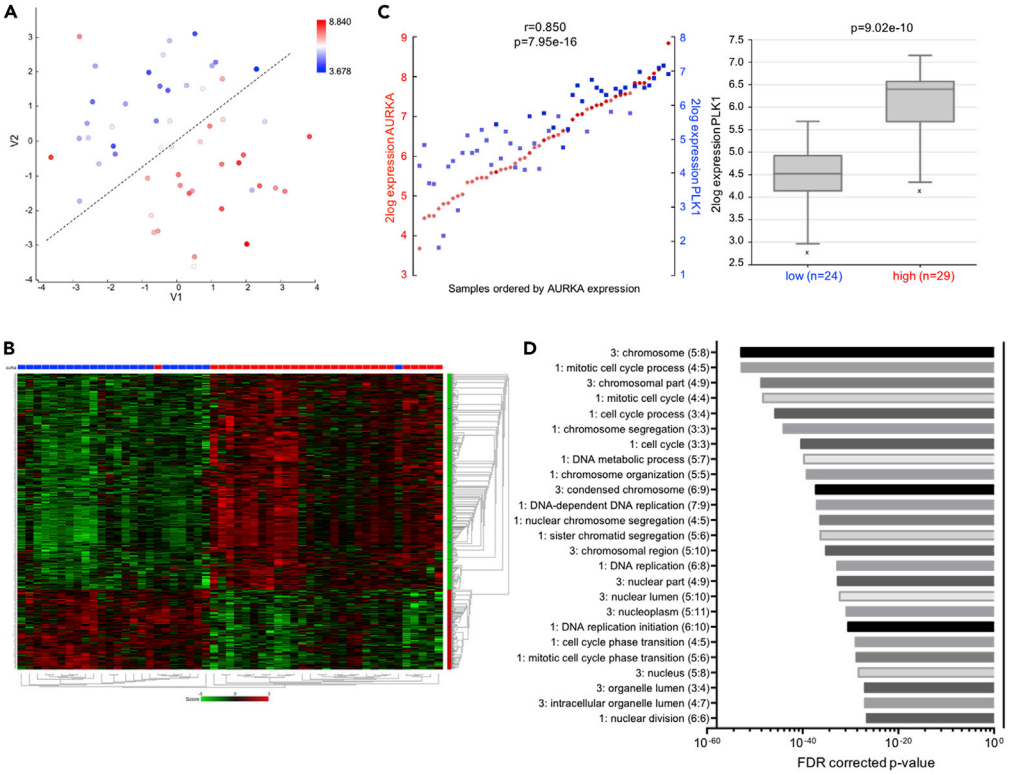

Figure 6. AURKA or PLK1 upregulation represents distinct molecular pHGG subgroups

(A) T-distributed stochastic neighbor embedding (t-SNE) clustering of 53 individual pHGG patient tumor samples (GSE: 19,578) (Paugh et al., 2010) based on genome-wide mRNA expression profiles (perplexity: 17). Samples are colored by their level (log2) of AURKA expression, with lower expression depicted in blue and higher expression in red.

(B) Hierarchical clustering analysis (*Z* score) of significantly differentially expressed genes between pHGG tissues with high (red) versus low (blue) AURKA mRNA expression levels, as selected by the dotted line in Figure 5A. Except for two samples (as shown in the top red and blue squared panel), high and low AURKA mRNA expression represent distinct molecular pHGG entities.

(C) Left panel: correlation between AURKA (in red) and PLK1 (in blue) (log2) mRNA expression levels in pHGG tissues. Right panel: Absolute difference of PLK1 mRNA expression between the high AURKA and low AURKA expressing subgroups as defined in Figure 5A mRNA expression differences between groups was tested using ANOVA. $p = 7.95 \times 10^{-16}$ (left) and $p = 9.02e^{-10}$ (right).

(D) Gene ontology (GO) analysis of genes selectively overexpressed in the subgroup of tumors with high AURKA mRNA expression defined in Figure 6A. Top 25 significantly enriched GO terms are shown, ranked according to FDR-corrected p value.

of the DNA-damage marker γH2AX, as is expected in cells that lose both NHEJ and HR. Notably, γH2AX expression increased upon treatment in responder (VUMC-DIPG-G, JHH-DIPG-01, and SU-DIPG-IV) but not in non-responder (VUMC-DIPG-10) DMG cultures, suggesting that cytotoxic synergism between PP and volasertib is related to an increase in DNA damage (Figure S10). Finally, we show increased cleaved-caspase 3 in all DMG models upon combination treatment, indicating activated apoptosis and suggesting, in part, regulated cell death (Figures 7C and S10). Altogether, these findings suggest that a subgroup of DMG highly depend on AURKA/PLK1 upregulation in order to move through cell cycle and control repair of DNA damage.

DISCUSSION

In this study, we identified AURKA as a potential therapeutic target in DMG, using kinome-wide CRISPR/Cas9 knockout screening. Subsequently, we used CRISPR/Cas9 synthetic lethality screening and identified PLK1 as a synergistic target to strengthen AURKA inhibition in DMG. We demonstrate that inhibition of PLK1 with volasertib, the most clinically advanced and selective small-molecule PLK1 inhibitor

CellPress
OPEN ACCESS

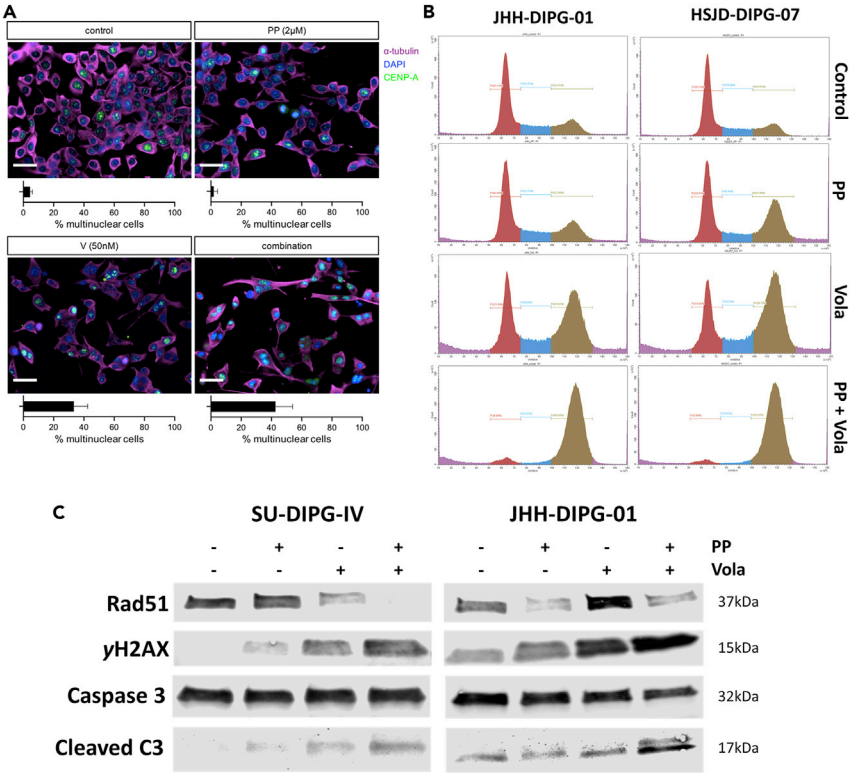

Figure 7. Combined inhibition of AURKA and PLK1 impairs cell division and induces DNA damage in DMG cells with AURKA/PLK1 overexpression

(A) Immunofluorescent stainings of α-tubulin (magenta), centromere protein A (CENP-A; green), and DAPI (blue) in SU-DIPG-IV cells after 24 h treatment with phthalazinone pyrazole (PP) (2μM), volasertib (V) (50nM), or the combination of both drugs. Quantification of multinuclear cell fractions is shown below the image, data are represented as average ±SD (based on ±1000 cells). Scale bar length is 60μm.

(B) Flow cytometry analysis for cell cycle distribution of the indicated DMG cells after 24 h treatment with PP, volasertib, or a combination thereof. The red peaks indicate G1-phase, the blue area S-phase, and the brown peaks G2-phase. All cells (including those in Figure S8) were treated with similar concentrations (5 μM PP and 30nM volasertib).

(C) Western blot analysis showing RAD51, γH2AX, caspase 3, and cleaved-caspase 3 protein expression in two representative DMG cultures after 48 h of treatment with phthalazinone pyrazole (PP), volasertib (Vola), or the combination of both drugs.

commercially available, synergizes with the AURKA inhibitor PP, a selective AURKA inhibitor that is predicted to passively crosses the blood-brain barrier (BBB) (Prime et al., 2011; Van den Bossche et al., 2016). Furthermore, we show that treatment synergy with volasertib is not unique to PP but can be recapitulated with alisertib, another selective AURKA inhibitor that is currently in phase 3 clinical trials (O'Connor et al., 2019), and through AURKA knockdown with shRNAs.

From RNA expression data and protein analyses, we observed that AURKA and PLK1 are concurrently overexpressed in DMG patient samples compared to healthy brain tissues and that expression of these proteins is predictive for tumor grade, prognosis, and *in vitro* PP/volasertib treatment sensitivity, corresponding to previous observations in these and other CNS malignancies (Alimova et al., 2017; Amani et al., 2016; Barton et al., 2010; Lens et al., 2010; Venkataraman et al., 2012). Our results further indicate that pediatric gliomas with overexpression of AURKA/PLK1 are specifically dependent on these mitotic regulators for cell division and prevention of DNA damage, which explains the preferential sensitivity to PP/volasertib combination therapy in these cells. While simultaneous targeting of AURKA and PLK1 has thus far not been studied in pHGG, including DMG, previous research in these tumors demonstrated that AURKA and PLK1 inhibitors, as monotherapy, induce double-strand DNA breaks, G2/M cell cycle arrest, and apoptosis, effects that are jointly indicative of chromosome instability during mitosis and are thereby in line with our findings (Alimova et al., 2017; Amani et al., 2016; Barton et al., 2010; Venkataraman et al., 2012).

Intriguingly, in a previously published kinome-wide functional genomic screen in DMG, using shRNA, AURKA was not among the top-hits identified (Silva-Evangelista et al., 2019). However, this shRNA screening was performed in adherently growing DMG cultures, which respond significantly different from drug treatment and harbor a differential expression profile compared to our non-adherent DMG neurosphere cultures (Meel et al., 2017). Furthermore, another study describes AURKB, but not AURKA, as relevant therapeutic target in DMG (Buczkowicz et al., 2013). In line with this study, we also identify AURKB as one of the top hits in DMG cells, albeit through a CRISPR/Cas9 knockout screen (Figure 1A). However, AURKB knockout also causes significant lethality in non-DMG control cells while AURKA knockout solely kills DMG cells, which suggests that AURKA is a less overall essential kinase and more DMG-specific therapeutic target.

It is well established that AURKA and PLK1 reciprocally activate each other and cooperatively regulate multiple stages of mitosis including mitotic entry, centrosome maturation, chromosome segregation, and cytokinesis, by phosphorylating shared or specific substrates (Asteriti et al., 2015; Joukov and De Nicolo, 2018; Lens et al., 2010). Based on these diverse functions, the molecular basis of synergism between PP and volasertib is likely to be multifaceted. For example, the antitumor synergism could be attributed to reduced phosphorylation of different substrates in certain mitotic stages. Alternatively, it could be due to altered phosphorylation of substrates common to both kinases (albeit on different phosphorylation sites). However, AURKA and PLK1 also perform a myriad of non-mitotic functions, i.e., suppressing apoptosis, regulating the DNA-damage response, promoting epithelial-mesenchymal transition (EMT), and stimulating the self-renewal capacity of cancer stem cells, suggesting that PP may not only acquire its antitumor synergism with volasertib by evoking mitotic defects (Fu and Wen, 2017; Harris et al., 2012; Ma and Poon, 2020; Mannino et al., 2014; Tang et al., 2017). For example, previous studies demonstrated that both AURKA and PLK1 are negative regulators of p53 and that depletion of these proteins results in G2/M arrest and apoptosis through reactivation of the p53 pathway (Liu, 2015; Ma and Poon, 2020; Tang et al., 2017). In our study, we did not observe a difference in PP/volasertib sensitivity based on TP53-mutational status, suggesting that p53 may not be implicated. Nonetheless, the precise molecular mechanism of synergy is yet to be fully elucidated, for example by more in-depth cell death analyses and investigation of mitotic regulators.

Accumulating evidence points to another role for AURKA and PLK1 as regulators of radio-resistance in pediatric brain tumors (Alimova et al., 2017; Amani et al., 2016; Barton et al., 2010; Gerster et al., 2010; Harris et al., 2012; Inoue et al., 2015; Rödel et al., 2010; Tandle et al., 2013; Tao et al., 2007; Venkataraman et al., 2012). In particular, PLK1 inhibitors have been shown to increase the radiosensitivity of these tumors by arresting cells at mitosis, which is the most radiosensitive cell cycle phase due to the relatively low amounts of DNA-repair proteins and antioxidants (Inoue et al., 2015). While simultaneous inhibition of AURKA and PLK1 has thus far not been evaluated as a radiosensitizing strategy, we demonstrate that PP/volasertib combination therapy increases DNA damage and impairs progression through mitosis, which alludes to the potential of a triple combination therapy with local radiation. PLK1 inhibitors may be particularly attractive in this regard as these have been shown to enhance glioma cell radiosensitivity without affecting non-transformed cells, suggesting that this radiosensitization strategy may be accompanied by minimal side effects (Tandle et al., 2013). As such, our results could serve as the basis for in-depth studies to the potential of AURKA/PLK1 inhibitor-mediated radiosensitization in DMG, which already receive radiotherapy as part of standard clinical care.

Successful treatment of CNS malignancies is often significantly obstructed by the BBB, which prevents most small-molecule inhibitors from reaching the tumor (Haumann et al., 2020). Although the integrity of the BBB is often intact in DMG, *in silico* analysis of the structure of PP shows that BBB penetration is feasible (Haumann et al., 2020). Furthermore, previous studies showed that alisertib penetrates pHGG xenografts in mouse brains, which will therefore be a relevant alternative to PP in future *in vivo* and clinical studies (Kogiso et al., 2018). Likewise, volasertib has been shown to effectively treat various CNS malignancies *in vivo*, suggesting that it does cross the BBB, albeit to a limited extent (Dong et al., 2018; Gjertsen and Schöffski, 2015; Higuchi et al., 2018). Finally, it is worth mentioning that promising drug delivery innovations emerged in recent years, like convection-enhanced delivery (CED) and sonoporation using high-intensity focused ultrasound (HIFU) combined with microbubbles, which allows us to disrupt or circumvent the BBB and thereby broaden the translational scope of this combination therapy (Haumann et al., 2020).

In conclusion, we demonstrate that combined AURKA and PLK1 inhibition strongly and synergistically reduces tumor growth of patient-derived DMG neurospheres. Furthermore, we show that AURKA and PLK1 are overexpressed in DMG patient samples compared to healthy brain tissues and that expression of these proteins is predictive for tumor grade, prognosis, and AURKA/PLK1 inhibitor sensitivity, signifying these proteins as potential therapeutic targets. Our findings suggest that DMG cells with overexpression of AURKA/PLK1 suffer from impaired cell division and increased DNA damage upon inhibition of these proteins, an effect that may also increase the radiosensitivity of these tumors. As such, our study advocates for the development of highly specific brain penetrable AURKA and PLK1 inhibitors and encourages the clinical investigation of AURKA/PLK1 inhibition as part of future multimodal treatment regimens for patients with DMG.

Limitations of the study

Although our study identifies the essentiality of AURKA and PLK1 for DMG survival, we did not test AURKA and PLK1 inhibition *in vivo*, which is an important step for clinical translation. Unfortunately, no clinically used AURKA inhibitors currently cross the BBB and the development of such inhibitors would greatly strengthen the translational potential of this study. Furthermore, CRISPR/Cas9 knockout screenings in healthy CNS control cultures, like primary astrocytes, are not yet possible due to the absence of stable glial cultures that can be effectively transduced. This forced us to use a pediatric ATRT culture as non-DMG control in the initial CRISPR screens, which is biologically suboptimal compared to nonmalignant control cells.

STAR★METHODS

Detailed methods are provided in the online version of this paper and include the following:

- KEY RESOURCES TABLE
- RESOURCE AVAILABILITY
  - Lead contact
  - Materials availability
  - Data and code availability
- EXPERIMENTAL MODEL AND SUBJECT DETAILS
  - Cell cultures
- METHOD DETAILS
  - Human mRNA expression datasets
  - Chemicals
  - CRISPR/Cas9
  - Cell-viability assays
  - Knockdown models
  - Western blotting
  - Immunofluorescent imaging
  - Cell cycle analysis
- QUANTIFICATION AND STATISTICAL ANALYSIS

SUPPLEMENTAL INFORMATION

Supplemental information can be found online at https://doi.org/10.1016/j.isci.2022.104398.

ACKNOWLEDGMENTS

The authors would like to acknowledge Madelaine van Mackelenbergh, from the Princess Maxima Center (Utrecht, Netherlands), for her assistance with figure preparation and graphic design. Funding was provided by the Children Cancer Free Foundation (KIKA, Netherlands), within project number 210.

AUTHOR CONTRIBUTIONS

D.S.M. and E.H. conceived and designed the project. D.S.M., A.D.C., M.H.M., and P.Wa. developed and validated the *in vitro* models used in the study. D.S.M., A.D.C., J.R.G., and P.Wa. performed the functional *in vitro* and western blotting.experiments. D.S.M. and M.B. provided patient-derived DMG tissues and performed immunohistochemical stainings. D.S.M., J.R.G., and P.Wa optimized and performed the CRISPR/Cas9 experiments. D.S.M. and A.D.C. performed *in silico* data analysis J.K. provided bioinformatical and

statistical expertise and support. G.J.L.K. and E.H. acquired funding and supervised the study. All authors contributed to writing the manuscript.

DECLARATION OF INTERESTS

The authors have no conflicts of interest to declare.

Received: October 25, 2021
Revised: January 18, 2022
Accepted: May 9, 2022
Published: June 17, 2022

REFERENCES

Alimova, I., Pierce, A.M., Harris, P., Donson, A., Birks, D.K., Prince, E., Balakrishnan, I., Foreman, N.K., Kool, M., Hoffman, L., et al. (2017). Targeting Polo-like kinase 1 in SMARCB1 deleted atypical teratoid rhabdoid tumor. Oncotarget *8*, 97290–97303. https://doi.org/10.18632/oncotarget.21932.

Amani, V., Prince, E.W., Alimova, I., Balakrishnan, I., Birks, D., Donson, A.M., Harris, P., Levy, J.M.M., Handler, M., Foreman, N.K., et al. (2016). Polo-like kinase 1 as a potential therapeutic target in diffuse intrinsic pontine glioma. BMC Cancer *16*, 647. https://doi.org/10.1186/s12885-016-2690-6.

Asteriti, I.A., De Mattia, F., and Guarguaglini, G. (2015). Cross-talk between AURKA and Plk1 in mitotic entry and spindle assembly. Front. Oncol. *5*, 283. https://doi.org/10.3389/fonc.2015.00283.

Barton, V.N., Foreman, N.K., Donson, A.M., Birks, D.K., Handler, M.H., and Vibhakar, R. (2010). Aurora kinase A as a rational target for therapy in glioblastoma. J. Neurosurg. Pediatr. *6*, 98–105. https://doi.org/10.3171/2010.3.Peds10120.

Berchtold, N.C., Cribbs, D.H., Coleman, P.D., Rogers, J., Head, E., Kim, R., Beach, T., Miller, C., Troncoso, J., Trojanowski, J.Q., et al. (2008). Gene expression changes in the course of normal brain aging are sexually dimorphic. Proc. Natl. Acad. Sci. U S A. *105*, 15605–15610. https://doi.org/10.1073/pnas.0806883105.

Birks, D.K., Donson, A.M., Patel, P.R., Dunham, C., Muscat, A., Algar, E.M., Ashley, D.M., Kleinschmidt-Demasters, B.K., Vibhakar, R., Handler, M.H., and Foreman, N.K. (2011). High expression of BMP pathway genes distinguishes a subset of atypical teratoid/rhabdoid tumors associated with shorter survival. Neuro-oncology *13*, 1296–1307. https://doi.org/10.1093/neuonc/nor140.

Buczkowicz, P., Hoeman, C., Rakopoulos, P., Pajovic, S., Letourneau, L., Dzamba, M., Morrison, A., Lewis, P., Bouffet, E., Bartels, U., et al. (2014). Genomic analysis of diffuse intrinsic pontine gliomas identifies three molecular subgroups and recurrent activating ACVR1 mutations. Nat. Genet. *46*, 451–456. https://doi.org/10.1038/ng.2936.

Buczkowicz, P., Zarghooni, M., Bartels, U., Morrison, A., Misuraca, K.L., Chan, T., Bouffet, E., Huang, A., Becher, O., and Hawkins, C. (2013). Aurora kinase B is a potential therapeutic target in pediatric diffuse intrinsic pontine glioma. Brain Pathol. *23*, 244–253. https://doi.org/10.1111/j.1750-3639.2012.00633.x.

Daina, A., and Zoete, V. (2016). A BOILED-egg to predict gastrointestinal absorption and brain penetration of small molecules. ChemMedChem *11*, 1117–1121. https://doi.org/10.1002/cmdc.201600182.

Dong, J., Park, S.Y., Nguyen, N., Ezhilarasan, R., Martinez-Ledesma, E., Wu, S., Henry, V., Piao, Y., Tiao, N., Brunell, D., et al. (2018). The polo-like kinase 1 inhibitor volasertib synergistically increases radiation efficacy in glioma stem cells. Oncotarget *9*, 10497–10509. https://doi.org/10.18632/oncotarget.24041.

Du, R., Huang, C., Liu, K., Li, X., and Dong, Z. (2021). Targeting AURKA in Cancer: molecular mechanisms and opportunities for Cancer therapy. Mol. Cancer *20*, 15. https://doi.org/10.1186/s12943-020-01305-3.

Fu, Z., and Wen, D. (2017). The emerging role of polo-like kinase 1 in epithelial-mesenchymal transition and tumor metastasis. Cancers *9*, 131. https://doi.org/10.3390/cancers9100131.

Gerster, K., Shi, W., Ng, B., Yue, S., Ito, E., Waldron, J., Gilbert, R., and Liu, F.F. (2010). Targeting polo-like kinase 1 enhances radiation efficacy for head-and-neck squamous cell carcinoma. Int. J. Radiat. Oncol. Biol. Phys. *77*, 253–260. https://doi.org/10.1016/j.ijrobp.2009.11.027.

Gjertsen, B.T., and Schöffski, P. (2015). Discovery and development of the Polo-like kinase inhibitor volasertib in cancer therapy. Leukemia *29*, 11–19. https://doi.org/10.1038/leu.2014.222.

Gleize, V., Alentorn, A., Connen de Kérillis, L., Labussière, M., Nadaradjane, A.A., Mundwiller, E., Ottolenghi, C., Mangesius, S., Rahimian, A., Ducray, F., et al. (2015). CIC inactivating mutations identify aggressive subset of 1p19q codeleted gliomas. Ann. Neurol. *78*, 355–374. https://doi.org/10.1002/ana.24443.

Gravendeel, L.A., Kouwenhoven, M.C., Gevaert, O., de Rooi, J.J., Stubbs, A.P., Duijm, J.E., Daemen, A., Bleeker, F.E., Bralten, L.B., Kloosterhof, N.K., et al. (2009). Intrinsic gene expression profiles of gliomas are a better predictor of survival than histology. Cancer Res. *69*, 9065–9072. https://doi.org/10.1158/0008-5472.Can-09-2307.

Harris, P.S., Venkataraman, S., Alimova, I., Birks, D.K., Donson, A.M., Knipstein, J., Dubuc, A., Taylor, M.D., Handler, M.H., Foreman, N.K., and Vibhakar, R. (2012). Polo-like kinase 1 (PLK1) inhibition suppresses cell growth and enhances radiation sensitivity in medulloblastoma cells. BMC cancer *12*, 80. https://doi.org/10.1186/1471-2407-12-80.

Haumann, R., Videira, J.C., Kaspers, G.J.L., van Vuurden, D.G., and Hulleman, E. (2020). Overview of current drug delivery methods across the blood-brain barrier for the treatment of primary brain tumors. CNS Drugs *34*, 1121–1131. https://doi.org/10.1007/s40263-020-00766-w.

Higuchi, F., Fink, A.L., Kiyokawa, J., Miller, J.J., Koerner, M.V.A., Cahill, D.P., and Wakimoto, H. (2018). PLK1 inhibition targets Myc-activated malignant glioma cells irrespective of Mismatch repair deficiency-mediated acquired resistance to temozolomide. Mol. Cancer Ther. *17*, 2551–2563. https://doi.org/10.1158/1535-7163.Mct-18-0177.

Ianevski, A., He, L., Aittokallio, T., and Tang, J. (2017). SynergyFinder: a web application for analyzing drug combination dose-response matrix data. Bioinformatics (Oxford, England) *33*, 2413–2415. https://doi.org/10.1093/bioinformatics/btx162.

Inoue, M., Yoshimura, M., Kobayashi, M., Morinibu, A., Itasaka, S., Hiraoka, M., and Harada, H. (2015). PLK1 blockade enhances therapeutic effects of radiation by inducing cell cycle arrest at the mitotic phase. Scientific Rep. *5*, 15666. https://doi.org/10.1038/srep15666.

Johung, T.B., and Monje, M. (2016). Diffuse intrinsic pontine glioma: new pathophysiological insights and emerging therapeutic targets. Curr. Neuropharmacol *15*, 88–97. https://doi.org/10.2174/1570159x14666160509123229.

Jones, C., Karajannis, M.A., Jones, D.T.W., Kieran, M.W., Monje, M., Baker, S.J., Becher, O.J., Cho, Y.J., Gupta, N., Hawkins, C., Hargrave, D., Haas-Kogan, D.A., Jabado, N., Li, X.N., Mueller, S., Nicolaides, T., Packer, R.J., Persson, A.I., Phillips, J.J., Simonds, E.F., Stafford, J.M., Tang, Y., Pfister, S.M., and Weiss, W.A. (2016). Pediatric high-grade glioma: biologically and clinically in need of new thinking. Neuro Oncol. *19*. now101–161. https://doi.org/10.1093/neuonc/now101.

Joukov, V., and De Nicolo, A. (2018). Aurora-PLK1 cascades as key signaling modules in the regulation of mitosis. Sci. Signaling *11*. https://doi.org/10.1126/scisignal.aar4195.

Kawaguchi, A., Yajima, N., Tsuchiya, N., Homma, J., Sano, M., Natsumeda, M., Takahashi, H., Fujii, Y., Kakuma, T., and Yamanaka, R. (2013). Gene expression signature-based prognostic risk score

in patients with glioblastoma. Cancer Sci. *104*, 1205–1210. https://doi.org/10.1111/cas.12214.

Kogiso, M., Qi, L., Braun, F.K., Injac, S.G., Zhang, L., Du, Y., Zhang, H., Lin, F.Y., Zhao, S., Lindsay, H., et al. (2018). Concurrent inhibition of neurosphere and Monolayer cells of pediatric glioblastoma by aurora A inhibitor MLN8237 predicted survival extension in PDOX models. Clin. Cancer Res. : official J. Am. Assoc. Cancer Res. *24*, 2159–2170. https://doi.org/10.1158/1078-0432.Ccr-17-2256.

Lens, S.M.A., Voest, E.E., and Medema, R.H. (2010). Shared and separate functions of polo-like kinases and aurora kinases in cancer. Nat. Rev. Cancer *10*, 825–841. https://doi.org/10.1038/nrc2964.

Li, J., Hong, M.J., Chow, J.P., Man, W.Y., Mak, J.P., Ma, H.T., and Poon, R.Y. (2015a). Co-inhibition of polo-like kinase 1 and Aurora kinases promotes mitotic catastrophe. Oncotarget *6*, 9327–9340. https://doi.org/10.18632/oncotarget.3313.

Li, W., Köster, J., Xu, H., Chen, C.-H., Xiao, T., Liu, J.S., Brown, M., and Liu, X.S. (2015b). Quality control, modeling, and visualization of CRISPR screens with MAGeCK-VISPR. Genome Biol. *16*, 281. https://doi.org/10.1186/s13059-015-0843-6.

Li, W., Xu, H., Xiao, T., Cong, L., Love, M.I., Zhang, F., Irizarry, R.A., Liu, J.S., Brown, M., and Liu, X.S. (2014). MAGeCK enables robust identification of essential genes from genome-scale CRISPR/Cas9 knockout screens. Genome Biol. *15*, 554. https://doi.org/10.1186/s13059-014-0554-4.

Liu, X. (2015). Targeting polo-like kinases: a promising therapeutic approach for cancer treatment. Translational Oncol. *8*, 185–195. https://doi.org/10.1016/j.tranon.2015.03.010.

Lowe, B.R., Maxham, L.A., Hamey, J.J., Wilkins, M.R., and Partridge, J.F. (2019). Histone H3 mutations: an updated view of their role in chromatin deregulation and cancer. Cancers (Basel) *11*, 660. https://doi.org/10.3390/cancers11050660.

Ma, H.T., and Poon, R.Y.C. (2020). Aurora kinases and DNA damage response. Mutat. Res. *821*, 111716. https://doi.org/10.1016/j.mrfmmm.2020.111716.

Mannino, M., Gomez-Roman, N., Hochegger, H., and Chalmers, A.J. (2014). Differential sensitivity of Glioma stem cells to Aurora kinase A inhibitors: implications for stem cell mitosis and centrosome dynamics. Stem Cel. Res. *13*, 135–143. https://doi.org/10.1016/j.scr.2014.05.001.

Marumoto, T., Hirota, T., Morisaki, T., Kunitoku, N., Zhang, D., Ichikawa, Y., Sasayama, T., Kuninaka, S., Mimori, T., Tamaki, N., et al. (2002). Roles of aurora-A kinase in mitotic entry and G2 checkpoint in mammalian cells. Genes Cells *7*, 1173–1182. https://doi.org/10.1046/j.1365-2443.2002.00592.x.

Meel, M.H., de Gooijer, M.C., Guillén Navarro, M., Waranecki, P., Breur, M., Buil, L.C.M., Wedekind, L.E., Twisk, J.W.R., Koster, J., Hashizume, R., et al. (2018a). MELK inhibition in diffuse intrinsic pontine glioma. Clin. Cancer Res. *24*, 5645–5657. https://doi.org/10.1158/1078-0432.Ccr-18-0924.

Meel, M.H., de Gooijer, M.C., Metselaar, D.S., Sewing, A.C.P., Zwaan, K., Waranecki, P., Breur, M., Buil, L.C.M., Lagerweij, T., Wedekind, L.E., et al. (2020). Combined therapy of AXL and HDAC inhibition reverses mesenchymal transition in diffuse intrinsic pontine glioma. Clin. Cancer Res. *26*, 3319–3332. https://doi.org/10.1158/1078-0432.Ccr-19-3538.

Meel, M.H., Metselaar, D.S., Waranecki, P., Kaspers, G.J.L., and Hulleman, E. (2018b). An efficient method for the transduction of primary pediatric glioma neurospheres. MethodsX *5*, 173–183. https://doi.org/10.1016/j.mex.2018.02.006.

Meel, M.H., Schaper, S.A., Kaspers, G.J.L., and Hulleman, E. (2018c). Signaling pathways and mesenchymal transition in pediatric high-grade glioma. Cell Mol Life Sci. *75*, 871–887. https://doi.org/10.1007/s00018-017-2714-7.

Meel, M.H., Sewing, A.P., Waranecki, P., Metselaar, D.S., Wedekind, L.E., Koster, J., van Vuurden, D.G., Kaspers, G.J.L., and Hulleman, E. (2017). Culture methods of diffuse intrinsic pontine glioma cells determine response to targeted therapies. Exp. Cell Res. *360*, 397–403. https://doi.org/10.1016/j.yexcr.2017.09.032.

Metselaar, D.S., Meel, M.H., Benedict, B., Waranecki, P., Koster, J., Kaspers, G.J.L., and Hulleman, E. (2019). Celastrol-induced degradation of FANCD2 sensitizes pediatric high-grade gliomas to the DNA-crosslinking agent carboplatin. EBioMedicine *50*, 81–92. https://doi.org/10.1016/j.ebiom.2019.10.062.

Mueller, S., Yang, X., Pal, S., Ermioian, R., Fox, E., Gajjar, A., Minard, C., Liu, X., Prem, K., Reid, J., et al. (2018). PDCT-04. Phase 1 trial of wee1 kinase inhibitor azd1775 combined with radiation therapy for children with newly diagnosed diffuse intrinsic pontine glioma: a report from the children's oncology group phase 1 pilot consortium (ADVL1217). Neuro-Oncology *20*, vi201. https://doi.org/10.1093/neuonc/noy148.834.

Murat, A., Migliavacca, E., Gorlia, T., Lambiv, W.L., Shay, T., Hamou, M.F., de Tribolet, N., Regli, L., Wick, W., Kouwenhoven, M.C., et al. (2008). Stem cell-related "self-renewal" signature and high epidermal growth factor receptor expression associated with resistance to concomitant chemoradiotherapy in glioblastoma. J. Clin. Oncol. *26*, 3015–3024. https://doi.org/10.1200/jco.2007.15.7164.

O'Connor, O.A., Özcan, M., Jacobsen, E.D., Roncero, J.M., Trotman, J., Demeter, J., Masszi, T., Pereira, J., Ramchandren, R., Beaven, A., et al. (2019). Randomized phase III study of alisertib or investigator's choice (selected single agent) in patients with Relapsed or Refractory peripheral T-cell lymphoma. J. Clin. Oncol. *37*, 613–623. https://doi.org/10.1200/jco.18.00899.

Paugh, B.S., Broniscer, A., Qu, C., Miller, C.P., Zhang, J., Tatevossian, R.G., Olson, J.M., Geyer, J.R., Chi, S.N., da Silva, N.S., et al. (2011). Genome-wide analyses identify recurrent amplifications of receptor tyrosine kinases and cell-cycle regulatory genes in diffuse intrinsic pontine glioma. J. Clin. Oncol. *29*, 3999–4006. https://doi.org/10.1200/jco.2011.35.5677.

Paugh, B.S., Qu, C., Jones, C., Liu, Z., Adamowicz-Brice, M., Zhang, J., Bax, D.A., Coyle, B., Barrow, J., Hargrave, D., et al. (2010). Integrated molecular genetic profiling of pediatric high-grade gliomas reveals key differences with the adult disease. J. Clin. Oncol. *28*, 3061–3068. https://doi.org/10.1200/jco.2009.26.7252.

Prime, M.E., Courtney, S.M., Brookfield, F.A., Marston, R.W., Walker, V., Warne, J., Boyd, A.E., Kairies, N.A., von der Saal, W., Limberg, A., et al. (2011). Phthalazinone pyrazoles as potent, selective, and orally bioavailable inhibitors of Aurora-A kinase. J. Med. Chem. *54*, 312–319. https://doi.org/10.1021/jm101346r.

Rödel, F., Keppner, S., Capalbo, G., Bashary, R., Kaufmann, M., Rödel, C., Strebhardt, K., and Spänkuch, B. (2010). Polo-like kinase 1 as predictive marker and therapeutic target for radiotherapy in rectal cancer. Am. J. Pathol. *177*, 918–929. https://doi.org/10.2353/ajpath.2010.100040.

Silva-Evangelista, C., Barret, E., Ménez, V., Merlevede, J., Kergrohen, T., Saccasyn, A., Oberlin, E., Puget, S., Beccaria, K., Grill, J., et al. (2019). A kinome-wide shRNA screen uncovers vaccinia-related kinase 3 (VRK3) as an essential gene for diffuse intrinsic pontine glioma survival. Oncogene *38*, 6479–6490. https://doi.org/10.1038/s41388-019-0884-5.

Spartà, A.M., Bressanin, D., Chiarini, F., Lonetti, A., Cappellini, A., Evangelisti, C., Evangelisti, C., Melchionda, F., Pession, A., Bertaina, A., et al. (2014). Therapeutic targeting of Polo-like kinase-1 and Aurora kinases in T-cell acute lymphoblastic leukemia. Cell Cycle (Georgetown, Tex.) *13*, 2237–2247. https://doi.org/10.4161/cc.29267.

Sun, L., Hui, A.M., Su, Q., Vortmeyer, A., Kotliarov, Y., Pastorino, S., Passaniti, A., Menon, J., Walling, J., Bailey, R., et al. (2006). Neuronal and glioma-derived stem cell factor induces angiogenesis within the brain. Cancer Cell *9*, 287–300. https://doi.org/10.1016/j.ccr.2006.03.003.

Tandle, A.T., Kramp, T., Kil, W.J., Halthore, A., Gehlhaus, K., Shankavaram, U., Tofilon, P.J., Caplen, N.J., and Camphausen, K. (2013). Inhibition of Polo-like Kinase 1 in Glioblastoma Multiforme Induces Mitotic Catastrophe and Enhances Radiosensitisation, *49* (European journal of cancer), pp. 3020–3028. https://doi.org/10.1016/j.ejca.2013.05.013.

Tang, A., Gao, K., Chu, L., Zhang, R., Yang, J., and Zheng, J. (2017). Aurora kinases: novel therapy targets in cancers. Oncotarget *8*, 23937–23954. https://doi.org/10.18632/oncotarget.14893.

Tao, Y., Zhang, P., Frascogna, V., Lecluse, Y., Auperin, A., Bourhis, J., and Deutsch, E. (2007). Enhancement of radiation response by inhibition of Aurora-A kinase using siRNA or a selective Aurora kinase inhibitor PHA680632 in p53-deficient cancer cells. Br. J. Cancer *97*, 1664–1672. https://doi.org/10.1038/sj.bjc.6604083.

Van den Bossche, J., Lardon, F., Deschoolmeester, V., De Pauw, I., Vermorken, J.B., Specenier, P., Pauwels, P., Peeters, M., and Wouters, A. (2016). Spotlight on volasertib: preclinical and clinical evaluation of a promising Plk1 inhibitor. Med. Res. Rev. *36*, 749–786. https://doi.org/10.1002/med.21392.

Venkataraman, S., Alimova, I., Tello, T., Harris, P.S., Knipstein, J.A., Donson, A.M., Foreman, N.K., Liu, A.K., and Vibhakar, R. (2012). Targeting

Aurora Kinase A enhances radiation sensitivity of atypical teratoid rhabdoid tumor cells. J. Neurooncol. *107*, 517–526. https://doi.org/10.1007/s11060-011-0795-y.

Wang, B., Wang, M., Zhang, W., Xiao, T., Chen, C.-H., Wu, A., Wu, F., Traugh, N., Wang, X., Li, Z., et al. (2019). Integrative analysis of pooled CRISPR genetic screens using MAGeCKFlute. Nat. Protoc. *14*, 756–780. https://doi.org/10.1038/s41596-018-0113-7.

Yadav, B., Wennerberg, K., Aittokallio, T., and Tang, J. (2015). Searching for drug synergy in complex dose-response landscapes using an interaction potency model. Comput. Struct. Biotechnol. J. *13*, 504–513. https://doi.org/10.1016/j.csbj.2015.09.001.

Yang, L., Zhou, Q., Chen, X., Su, L., Liu, B., and Zhang, H. (2016). Activation of the FAK/PI3K pathway is crucial for AURKA-induced epithelial-mesenchymal transition in laryngeal cancer. Oncol. Rep. *36*, 819–826. https://doi.org/10.3892/or.2016.4872.

Yata, K., Lloyd, J., Maslen, S., Bleuyard, J.Y., Skehel, M., Smerdon, S.J., and Esashi, F. (2012). Plk1 and CK2 act in concert to regulate Rad51 during DNA double strand break repair. Mol. Cell *45*, 371–383. https://doi.org/10.1016/j.molcel.2011.12.028.

Yau, E.H., and Rana, T.M. (2018). Next-generation sequencing of genome-wide CRISPR screens. Methods Mol. Biol. *1712*, 203–216. https://doi.org/10.1007/978-1-4939-7514-3_13.

Zhang, L., Chen, L.H., Wan, H., Yang, R., Wang, Z., Feng, J., Yang, S., Jones, S., Wang, S., Zhou, W., et al. (2014). Exome sequencing identifies somatic gain-of-function PPM1D mutations in brainstem gliomas. Nat. Genet. *46*, 726–730. https://doi.org/10.1038/ng.2995.

Zhao, X., Wei, C., Li, J., Xing, P., Li, J., Zheng, S., and Chen, X. (2017). Cell cycle-dependent control of homologous recombination. Acta Biochim. Biophys. Sin (Shanghai) *49*, 655–668. https://doi.org/10.1093/abbs/gmx055.

Dull, T., Zufferey, R., Kelly, M., Mandel, R.J., Nguyen, M., Trono, D., and Naldini, L. (1998). A third-generation lentivirus vector with a conditional packaging system. J. Virol. *72*, 8463–8471. https://doi.org/10.1128/jvi.72.11.8463-8471.1998.

Wang, T., Wei, J.J., Sabatini, D.M., and Lander, E.S. (2014). Genetic screens in human cells using the CRISPR-Cas9 system. Science *343*, 80–84. https://doi.org/10.1126/science.1246981.

CellPress
OPEN ACCESS

STAR★METHODS

KEY RESOURCES TABLE

REAGENT or RESOURCE	SOURCE	IDENTIFIER
Antibodies		
mouse anti-phospho-Histone H2A.X (Ser139)	Millipore	#05-636; RRID: AB_309864
rabbit anti-RAD51 (D4B10)	Cell Signaling Technology	#8875s; RRID: AB_2721109
rabbit anti-AURKA (D3E4Q)	Cell Signaling Technology	#14475; RRID: AB_2665504
rabbit anti-PLK1 (208G4)	Cell Signaling Technology	#4513; RRID: AB_2167409
rabbit anti-Caspase 3	Cell Signaling Technology	#9662S; RRID: AB_331439
rabbit anti-Cleaved Caspase 3 (D175)	Cell Signaling Technology	#9661S; RRID: AB_2341188
mouse anti-β actin (Clone C4)	Millipore	#MAB1501; RRID: AB_2223041
goat anti-mouse IRDye©680RD	LI-COR	#926-68070; RRID: AB_10956588
goat anti-rabbit IRDye©800CW	LI-COR	#926-32211; RRID: AB_621843
mouse anti-α-Tubulin (DM1A)	Sigma-Aldrich	#T9026; RRID: AB_477593
rabbit anti-CENP-A	Cell Signaling Technology	#2186; RRID: AB_10828491
goat anti-mouse Alexa Fluor™ 488	Thermo Fisher Scientific	#A-11029; RRID: AB_2534088
goat anti-rabbit Alexa Fluor™ 594	Thermo Fisher Scientific	#A-11037; RRID: AB_2534095
Bacterial and virus strains		
NEB® 5-alpha Competent *E. coli*	New England Biolabs	C2987H
pRSV-Rev lentiviral packaging plasmid (3rd gen)	(Dull et al., 1998)	Addgene: #12253
pMDLg/pRRE lentiviral packaging plasmid (3rd gen)	(Dull et al., 1998)	Addgene: #12251
pMD2.G lentiviral envelope plasmid (3rd gen)	(Dull et al., 1998)	Addgene: #12259
Biological samples		
Autopsy-derived pediatric diffuse midline glioma tissues	Pathology dept. Amsterdam UMC / Netherlands Brain bank	Protcol: METC VUmc 2009/237
Chemicals, peptides, and recombinant proteins		
Phthalazinone pyrazole	Cayman Chemical Company	Cat No. 10735 / CAS: 880487-62-7
Volasertib (BI 6727)	Selleck Chemicals	Cat No. S2235 / CAS: 755038-65-4
PH-797804	Selleck Chemicals	Cat. No. S2726 / CAS: 586379-66-0
Fasudil (HA-1077) HCl	Selleck Chemicals	Cat No. S1573 / CAS: 105628-07-7
Y-27632 2HCl	Selleck Chemicals	Cat No. S1049 / CAS: 129830-38-2
Alisertib (MLN8237)	Selleck Chemicals	Cat No. S1133 / CAS: 1028486-01-2
Birabresib (OTX015)	MedChemExpress	Cat No. HY-15743 / CAS: 202590-98-5
Critical commercial assays		
CellTiter-Glo® 3D Luminescent Cell Viability Assay	Promega	#G9683
GeneJET Gel Extraction Kit	Thermo Fisher Scientific	#K0691
Deposited data		
All RNAseq datasets used in this manuscript are described in Table S2	This paper	N/A
Experimental models: Cell lines		
Human: VUMC-DIPG-10 (pediatric DMG cells)	Laboratory of Esther Hulleman	Accession: CVCL_IT43
Human: SU-pcGBM2 (pediatric GBM cells)	Laboratory of Michelle Monje	Accession: CVCL_IT42

(*Continued on next page*)

Continued

REAGENT or RESOURCE	SOURCE	IDENTIFIER
Human: SU-DIPG-IV (pediatric DMG cells)	Laboratory of Michelle Monje	Accession: CVCL_IT39
Human: SU-DIPG-XXI (pediatric DMG cells)	Laboratory of Michelle Monje	N/A
Human: HSJD-DIPG-07 (pediatric DMG cells)	Laboratory of Montero Carcaboso	Accession: CVCL_VU70
Human: VUMC-DIPG-G (pediatric DMG cells)	Laboratory of Esther Hulleman	N/A
Human: JHH-DIPG-1 (pediatric DMG cells)	Laboratory of Eric Raabe	Accession: CVCL_IT47
Human: VUMC-ATRT-03 (pediatric ATRT cells)	Laboratory of Esther Hulleman	N/A
Human: VUMC-ATRT-01 (pediatric ATRT cells)	Laboratory of Esther Hulleman	N/A
Human: HEK 293t (adult embryonal kidney cells)	ATCC	CRL-3216
Oligonucleotides		
Short hairpin targeting AURKA #1, TTGTAGGTCTCTTGGTATGTG	Horizon, PerkinElmer	Clone TRCN0000010533
Short hairpin targeting AURKA #2, TATAAGTAGCACAATTCTCGT	Horizon, PerkinElmer	Clone TRCN0000000655
Short hairpin targeting AURKA #3, ATTCCAGAATTAGGTAGACTC	Horizon, PerkinElmer	Clone TRCN0000000657
Short hairpin targeting PLK1 #1, ACCTGCAAGGATGATGCAGCT	Horizon, PerkinElmer	Clone TRCN0000011006
Short hairpin targeting PLK1 #2, AACTCGTCATTAAGCAGCTCG	Horizon, PerkinElmer	Clone TRCN0000121073
Short hairpin targeting PLK1 #3, AAGCAGCTCGTTAATGGTTGG	Horizon, PerkinElmer	Clone TRCN0000006246
sgRNA amplification primer FW, GCCGGCTCGAGTGTACAAAA	This paper	N/A
sgRNA amplification primer RV, AGCGCTAGCTAATGCCAACTT	This paper	N/A
Recombinant DNA		
Human CRISPR knockout pooled library (kinome-wide)	(Wang et al., 2014)	Addgene: #51044
pCW-Cas9 (doxycycline inducible, puromycin resistance)	(Wang et al., 2014)	Addgene: #50661
Software and algorithms		
MAGeCK-VISPR algorithm *(comprehensive quality control, analysis, and visualization workflow for CRISPR/Cas9 screens)*	Developed by Wei Li and Han Xu from Xiaole Shirley Liu's lab	https://bitbucket.org/liulab/mageck-vispr/src/master/
MAGeCKFlute R package version 1.14.0 *(Integrative Analysis Pipeline for Pooled CRISPR Functional Genetic Screens)*	Developed by Binbin Wang, Wubing Zhang, Feizhen Wu, Wei Li & X. Shirley Liu	https://www.bioconductor.org/packages/release/bioc/html/MAGeCKFlute.html
R2: Genomics Analysis and Visualization Platform	Established by Jan Koster	https://hgserver2.amc.nl/
MARS Data Analysis Software	BMG LABTECH	ID: # 81306
LAS X Life Science Microscope Software Platform	Leica	https://www.leica-microsystems.com
CytExpert 2.3.0.84 software package	Beckman Coulter	https://www.mybeckman.nl/flow-cytometry
Other		
Tecan D300e picoliter dispenser	Tecan Group	N/A
Cell-repellent 96-well F-bottom plates	Greiner Bio-one	#650971

(*Continued on next page*)

CellPress
OPEN ACCESS

Continued

REAGENT or RESOURCE	SOURCE	IDENTIFIER
Cell-repellent 96-well U-bottom plates	Greiner Bio-One	#650970
SCREENSTAR® 96-well plates	Greiner Bio-One	#655-866
Illumina NovaSeq 6000 sequencing system	Illumina	N/A

RESOURCE AVAILABILITY

Lead contact

Further information and requests for resources and reagents should be directed to and will be fulfilled by the lead contact, dr. Esther Hulleman (e.hulleman@prinsesmaximacentrum.nl).

Materials availability

This study did not generate new unique reagents.

Data and code availability

- All the detailed data in this paper are available upon request.
- This paper does not report original code.
- Any additional information required to reanalyze the data reported in this paper is available from the lead contact upon request

EXPERIMENTAL MODEL AND SUBJECT DETAILS

Cell cultures

The human primary cell lines VUMC-DIPG-10 (H3-wildtype), VUMC-DIPG-G (H3.3K27M), VUMC-ATRT-01 (sonic hedgehog subtype), and VUMC-ATRT-03 (sonic hedgehog subtype) were established from autopsy or resection material at the Amsterdam UMC (Amsterdam, the Netherlands), as previously described (Meel et al., 2017). HSJD-DIPG-07 (H3.3K27M) was a kind gift from Dr. Montero Carcaboso (Hospital San Joan de Deu, Barcelona, Spain), JHH-DIPG-01 (H3.3K27M) from Dr. Raabe (John Hopkins Hospital, Baltimore, MD, USA), and SU-DIPG-IV (H3.1K27M), SU-DIPG-XXI (H3.1K27M) and SU-pcGBM2 (H3-wildtype GBM) from Dr. Monje (Stanford University, Stanford, CA, USA). An overview, including details on the molecular background and treatment history, of all the models used in this study is depicted in Table S1.

All cells were cultured as neurospheres at 37°C and 5% CO_2 in modified Tumor Stem Medium (TSM), consisting of 48% Neurobasal-A medium, 48% DMEM/F12, 1% HEPES 1M, 1% MEM non-essential amino acids, 1% Sodium Pyruvate 100 mM, 1% GlutaMAX, and 1% penicillin/streptomycin (i.e. TSM base), supplemented with 2% B27, 1% N2 (all purchased from ThermoFisher Scientific, Waltham, MA, USA), 20 ng/mL human EGF, 20 ng/mL human bFGF, 10 ng/mL human PDGF-AA, 10 ng/mL human PDGF-BB (Peprotech, London, UK), and 5 IU/mL heparin (Amsterdam UMC pharmacy, Amsterdam, the Netherlands) (i.e. complete TSM). All cell lines were authenticated by short tandem-repeat (STR) profiling to ensure cell identity and only used when confirmed mycoplasma negative.

Human fetal primary astrocytes (#1800, ScienCell Research Laboratories, Carlsbad, CA, USA) were cultured in ScienCell medium supplemented with FBS, P/S and Astrocyte Growth Supplement (all ScienCell Research Laboratories) at 37°C and 5% CO_2.

METHOD DETAILS

Human mRNA expression datasets

Expression datasets used in this study to compare mRNA expression between patients were the following: healthy brain (GSE: 11882) (Berchtold et al., 2008), pediatric glioma (GSE: 19578) (Paugh et al., 2010), pediatric DMG (GSE: 26576) (Paugh et al., 2011), ATRT (GSE: 28026) (Birks et al., 2011), adult glioma (GSE: 16011, 43378, 50774, 7696, 4290) (Gleize et al., 2015; Gravendeel et al., 2009; Kawaguchi et al., 2013; Murat et al., 2008; Sun et al., 2006; Zhang et al., 2014). These datasets were accessed through the R2 Genomics Platform (http://r2.amc.nl), a database that includes gene expression profiles from large patient cohorts,

including tools to compare gene expression between different cancer types. Normalization of the mRNA expression datasets was conducted using the MAS5.0 algorithm. All datasets used in this manuscript are summarized and specified in Table S2.

Chemicals

Phthalazinone pyrazole was purchased from Cayman Chemical Company (Ann Arbor, MI, USA), volasertib (BI 6727), losmapimod (GW856553X), PH-797804, fasudil (HA-1077) HCl, Y-27632 2HCl, and alisertib (MLN8237) were purchased from Selleck Chemicals (Houston, TX, USA). Birabresib (OTX015) was purchased from MedChemExpress (Monmouth, NJ, USA). All chemicals were dissolved in DMSO and stored as 10mM stock at −20°C.

CRISPR/Cas9

VUMC-DIPG-10, HSJD-DIPG-07, and VUMC-ATRT-03 cells were stably transduced with the doxycycline inducible pCW-Cas9 plasmid as previously described (Meel et al., 2018b). pCW-Cas9 was a gift from Eric Lander & David Sabatini (Addgene plasmid #50661). The transduced cells were selected with 2 μg/mL puromycin (#A1113802, ThermoFisher Scientific, Waltham, USA) for 48h. pCW-Cas9 expressing VUMC-DIPG-10, HSJD-DIPG-07, and VUMC-ATRT-03 cells were stably transduced (Meel et al., 2018b) with the Human CRISPR enriched pooled kinase gRNA sub-pool library at an MOI of 0.3 and at 500-fold coverage of the library. The transduced cells were selected with 15 μg/mL blasticidin (#203350, Sigma-Aldrich) for 7 days. Human CRISPR enriched pooled kinase gRNA sub-pool library was a gift from David Sabatini & Eric Lander (Addgene #51044). CRISPR-Cas9 screens were performed according to the protocol published by Yao and Rana (Yau and Rana, 2018), with scaling down of number of transduced cells and subsequent PCRs to account for the smaller size of the human kinase gRNA sub-pool library. A minimum of 12.5*10 6 cells were taken at day 0, day 14, and day 21. Cell pellets were dissolved in 1.5mL TRIzol™ Reagent (#15596026, Invitrogen, Waltham, USA) and genomic DNA was harvested from the samples according to the TRIzol™ Reagent User Guide (Invitrogen). 5 μg of extracted genomic DNA from each sample was used as a template for 4 × 100 μL PCR reactions with 17 cycles using NEBNext High Fidelity Q5 Polymerase (#M0491L, New England Biolabs, Ipswich, USA) and primers with sequences:

5′- GCCGGCTCGAGTGTACAAAA -3′ (Outer Forward)

5′- AGCGCTAGCTAATGCCAACTT -3′ (Outer Reverse)

were used to amplify the sgRNA region. Samples were gel extracted using a GeneJET Gel Extraction Kit (#K0691, ThermoFisher Scientific). The PCR products for each sample were pooled and 10 μL used as a template for a second PCR with 12 cycles to attach sequencing adaptors. Samples were quantified using a BioAnalyzer 2100 Expert (Agilent Technologies, Santa Clara, USA) and DNA 7500 Kit (Agilent Technologies). Amplified DNA was sequenced using an Illumina NovaSeq 6000 sequencing system (Illumina, San Diego, USA) at a minimum depth of 68 million reads/sample. Fastq.gz sequencing files were analysed using the MAGeCK-VISPR algorithm (Li et al., 2014, 2015b). MAGeCK-VISPR performs quality control, sgRNA counting and generation of a maximum likelihood estimation (mle) of gene essentiality (β-score) for each gene in the kinase library with associate p value and FDR-value. Generated mle files were uploaded to the MAGeCKFlute R package (Wang et al., 2019) in RStudio (Rstudio, PBC) were they were cell-cycle normalized using the Zuber Essential Gene List.

Cell-viability assays

Neurospheres were dissociated by incubation in Accutase (#00-4555-56, ThermoFisher Scientific, Waltham, MA, USA) for 5 min at 37°C, followed by mild mechanical dissociation by pipetting. Accutase was inactivated in TSM base, after which cells were resuspended in complete TSM and filtered through a 100μm cell strainer to generate a single-cell suspension. Cells were plated at a density of 1000–5000 cells/well, depending on growth rate, in complete TSM in cell-repellent 96-well F-bottom (#650971) or U-bottom plates (#650970, Greiner Bio-one, Kremsmünster, Austria). 500 cells/well were used for long-term assays to avoid growth inhibition as the result of confluency. Compounds were dispersed 24h after cell seeding using a Tecan D300e picoliter dispenser (Tecan Group Ltd, Switzerland). For short-term assays, the number of viable cells was measured after 96h using the CellTiter-Glo® 3D Luminescent Cell Viability Assay (#G9683, Promega, Madison, USA) according to the manufacturer's protocol. The concordant luminescence was measured using a FLUOstar® Omega microplate reader (BMG LABTECH, Offenburg, Germany) operated

by MARS data analysis software. For long-term assays, treatment was withdrawn after 96h drug incubation and regrowth of neurospheres was monitored for 10 days, with culture medium refreshed twice per week. After 10 days, phase-contrast images were taken using a Leica DMi8 inverted microscope (Leica Microsystems, Wetzlar, Germany) operated by LAS X Navigator Software, and cell viability was measured, as described above.

Knockdown models

AURKA and PLK1 knockdown cells were established using lentiviral transduction with the pLKO.1-shAURKA.1, pLKO.1-shAURKA.2, pLKO.1-shAURKA.3, pLKO.1-shPLK1.1, pLKO.1-shPLK1.2, and pLKO.1-shPLK1.3 plasmids (Horizon™, PerkinElmer) as described previously (Metselaar et al., 2019). shRNA sequences are summarized in Table S3.

Western blotting

Cells were harvested under optimal growth conditions or after 48h exposure to the indicated drugs, washed with ice-cold PBS, and snap-frozen in liquid nitrogen. Frozen cell pellets were lysed for 1h at 4°C in RIPA buffer (1% NP-40, 0.5% sodium deoxycholate, 0.1% SDS, 50mM Tris HCl pH 7.6, 150mM NaCl) supplemented with 50mM β-glycerolphosphate, 1mM DTT, 1x cOmplete™ Mini EDTA-free Protease Inhibitor Cocktail, and 1 mM Na_3VO_4 (all purchased from Sigma Aldrich, Saint Louis, MO, USA). Protein concentration was measured using the Bio-Rad Protein Assay Kit (#5000001, BioRad, Hercules, CA, USA) and a SPECTROstar® Nano microplate reader (BMG LABTECH, Offenburg, Germany) operated by MARS data analysis software. Normalized protein samples were reduced using NuPAGE™ LDS Sample Buffer (#NP0007, ThermoFisher Scientific, Waltham, MA, USA). 50μg protein per sample and the PageRuler™ Plus Prestained Protein Ladder (#26620, Thermo Fisher, Waltham, MA, USA) were separated by gel electrophoresis using 4–20% Mini-PROTEAN® TGX™ Precast Protein Gels (#4561094) and transferred using the Trans-Blot Turbo Mini 0.2 μm Nitrocellulose Transfer Pack (#1704158) and the Trans-Blot® Turbo Transfer System (all purchased from BioRad, Hercules, CA, USA). Membranes were blocked for 30min in Blocking Buffer for Fluorescent Western Blotting (#MB-070, Rockland®, PA, USA), and incubated overnight at 4°C with the indicated primary antibodies. Primary antibodies included: mouse anti-phospho-Histone H2A.X (Ser139) (1:1000, #05–636, Millipore, Burlington, MA, USA), rabbit anti-RAD51 (D4B10) (1:1000, #8875s, Cell Signaling Technology, Danvers, MA, USA), rabbit anti-AURKA (D3E4Q) (1:1000, #14475, Cell Signaling Technology), rabbit anti-PLK1 (208G4) (1:1000, #4513, Cell Signaling Technology), rabbit anti-Caspase 3 (1:1000, #9662S, Cell Signaling Technology), rabbit anti-Cleaved Caspase 3 (D175) (1:1000, #9661S, Cell Signaling Technology), and mouse anti-β actin (Clone C4) (1:5000, #MAB1501, Millipore). After overnight incubation, membranes were washed and incubated with secondary goat anti-mouse IRDye©600CV antibody (1:5000, LI-COR©, Lincoln, NA, USA) and/or goat anti-rabbit IRDye©800CV antibody (1:5000, LI-COR©). Protein detection was performed using an LI-COR© Oddyssey fluorescent imager (Model 9120; Surplus Solutions, LLC).

Immunofluorescent imaging

After generating a single cell suspension, SU-DIPG-IV cells were plated at a density of 5000 cells/well in complete TSM in SCREENSTAR® 96-well plates (#655–866, Greiner Bio-one, Kremsmünster, Austria) specialized for fluorescent imaging. Compounds were dispersed 24h after cell seeding using the Tecan D300e picoliter dispenser. After 24h, cells were fixed with 4% paraformaldehyde for 15min and permeabilized using 0.25% Triton-X100 for 10min. Non-specific binding was blocked by incubating with Normal Antibody Diluent (Phosphate Buffered) (ScyTek Laboratories, Logan, UT, USA) for 15min. Primary antibody incubation was performed overnight at 4°C using mouse anti-α-Tubulin (DM1A) (1:250, #T9026, Sigma-Aldrich, Saint Louis, MO, USA) and rabbit anti-CENP-A (1:200, #2186, Cell Signaling Technology, Danvers, MA, USA). After overnight incubation, the cells were incubated with the secondary goat anti-mouse Alexa Fluor™ 488 antibody (1:500, #A-11029, ThermoFisher Scientific, Waltham, MA, USA) and goat anti-rabbit Alexa Fluor™ 594 antibody (1:500, #A-11037, ThermoFisher Scientific, Waltham, MA, USA) for 1h and then counterstained with 300nM DAPI (#D1306, ThermoFisher Scientific, Waltham, MA, USA) for 5min. Imaging was performed using the Leica DMi8 inverted microscope, including motorized scanning stage. Quantification of the multinuclear cells has been performed manually by an independent researcher. For each condition an overview image was created through automated stage stitching microscopy. From these images and for each condition, ten random squares were selected containing 50–100 cells. In each square, the total amount of single-nuclear and multinuclear cells was manually counted to establish percentages.

Cell cycle analysis

Cells were treated for 48h with the indicated compounds and subsequently made single cell as earlier described. Cells were resuspended in 4mL TSM and pulled through a 100μm cell strainer to secure all cells being singlets. Cells were counted and, if needed, adjusted to less than one million cells per mL. Hoechst33342 (5 μg/mL) was added to the cell suspension and incubated for 1h at 37°C. Cells were pulled through a FACS strainer to remove clumps, centrifuged, and resuspended in 200-300μL PBS. Cell cycle analysis was performed on a CytoFLEX LX Flow Cytometer (Beckman Coulter, Inc.) using a UV450 nm filter. Software analysis was performed using the CytExpert 2.3.0.84 software package (Beckman Coulter, Inc.).

QUANTIFICATION AND STATISTICAL ANALYSIS

All *in vitro* data are represented as averages (mean ± s.d.) from at least three technical replicates. *In vitro* cell survival percentages were compared using the one-way analysis of variance (ANOVA) and post-hoc unpaired, two-tailed student's t-tests with Bonferroni correction. Synergy scores are based on the average percentage viability and were calculated using the Zero interaction potency (ZIP) model of the SynergyFinder software (http://synergyfinder.fimm.fi) (Ianevski et al., 2017; Yadav et al., 2015). mRNA expression between groups from *in silico* R2 analyses was assessed using ANOVA. *In silico* survival differences between groups were tested using the log rank (Mantel-Cox) test. Analyses were performed using GraphPad Prism (version 8.0.2, GraphPad Software, Inc) or Microsoft Excel (version 14.7.2). p-values below 0.05 (two-sided) were considered statistically significant.